

Accepted refereed manuscript of:

Wang S, Li J, Zhang B, Spyrakos E, Tyler AN, Shen Q, Zhang F, Kuster T, Lehmann MK, Wu Y & Peng D (2018) Trophic state assessment of global inland waters using a MODIS-derived Forel-Ule index. *Remote Sensing of Environment*, 217, pp. 444-460.

DOI: [10.1016/j.rse.2018.08.026](https://doi.org/10.1016/j.rse.2018.08.026)

©2018, Elsevier. Licensed under the Creative Commons Attribution-NonCommercial-NoDerivatives 4.0 International  
<http://creativecommons.org/licenses/by-nc-nd/4.0/>



24 natural water colour into 21 indices from dark blue to yellowish-brown. Then the  
25 relationship between FUI and the trophic state index (TSI) was established based on in-  
26 situ measurements and MODIS products. The water-leaving reflectance at 645 nm band  
27 was employed to distinguish coloured dissolved organic matter (CDOM)-dominated  
28 systems in the FUI-based trophic state assessment. Based on the analysis, the FUI-based  
29 trophic state assessment method was developed and applied to assess the trophic states  
30 of 2058 large inland water bodies (surface area > 25 km<sup>2</sup>) distributed around the world  
31 using MODIS data from the austral and boreal summers of 2012. Our results showed  
32 that FUI can be retrieved from MODIS with a considerable accuracy (92.5%, R<sup>2</sup>=0.92)  
33 by comparing with concurrent in situ measurements over a wide range of lakes, and the  
34 overall accuracy of the FUI-based trophic state assessment method is 80.0% (R<sup>2</sup> = 0.75)  
35 validated by an independent dataset. Of the global large water bodies considered,  
36 oligotrophic large lakes were found to be concentrated in plateau regions in central Asia  
37 and southern South America, while eutrophic large lakes were concentrated in central  
38 Africa, eastern Asia, and mid-northern and southeast North America.

39 **Keywords:** trophic state, global inland waters, Forel-Ule index, MODIS

## 40 **1. Introduction**

41 Eutrophication represents a serious water quality challenge around the world  
42 (Jones and Lee, 1982; Le et al., 2010; Smith, 2003; Vollenweider, 1981). This process  
43 is often associated with the rapid production of phytoplankton and other  
44 microorganisms, which have important impacts on aquatic ecology and the normal  
45 functioning of water bodies (Vollenweider and Kerekes, 1982). The trophic state of  
46 inland waters is typically categorized into three levels: oligotrophic, mesotrophic, and  
47 eutrophic. Since the 1960s, attempts have been made to quantitatively evaluate the  
48 trophic state of inland waters using both single-variable and multi-variable methods  
49 (Beeton and Edmondson, 1972; Bigham Stephens et al., 2015; Burns and Bryers, 2000;  
50 Forsberg and Ryding, 1980; Rodhe, 1969). Carlson (1977) introduced a numerical  
51 *Trophic State Index* (TSI) for inland waters based on algae biomass, which can be  
52 calculated using Secchi depth (SD), chlorophyll-a (Chl-a), or total phosphorus (TP).  
53 Many studies have used Chl-a, a pigment common to almost all photosynthetic  
54 organisms, as a proxy for algal biomass and therefore also as an indicator for the trophic  
55 state of aquatic systems (Carlson, 1991; Joniak et al., 2009; Sheela et al., 2011a). The  
56 Trophic Level Index (TLI), another commonly used numerical method, is calculated  
57 from the weighted sum of either three variables (Chl-a, TP, total nitrogen (TN)) or five  
58 variables with the addition of SD and chemical oxygen demand (COD) (Burns and  
59 Bryers, 2000; Burns et al., 1999; Jin and Tu, 1990; Verburg et al., 2010).

60 Collecting systematic observations on the ecological status of inland waters in  
61 aquatic systems in inland waters remains a logistical and financial challenge which with  
62 conventional in-situ approaches scales proportionately with increasing geographical  
63 coverage (Härmä et al., 2001; Hu et al., 2010; McClain, 2009). However, satellite based  
64 remote sensing (RS) offers a potentially significant source of information for large-  
65 scale monitoring of water state variables (including water trophic state).

66 Eutrophication and increased productivity typically result in changes in the optical  
67 properties of water; therefore, RS approaches have been employed for water trophic  
68 state assessment (Baban, 1996; Papoutsas et al., 2014), in particular through the retrieval  
69 of Chl-a concentrations (Chen, 2003; Duan et al., 2007; Matthews and Odermatt, 2015;  
70 Pulliainen et al., 2001; Thiemann and Kaufmann, 2000; Wang et al., 2008). In addition,  
71 SD, which is one of the most commonly measured trophic state indicators, has also  
72 been used to assess water trophic states (Binding et al., 2015; Knight and Voth, 2012;  
73 Lillesand et al., 1983; Olmanson et al., 2008; Papoutsas et al., 2014; Sheela et al., 2011b).  
74 Other studies based on RS have used multiple variables to assess water trophic states  
75 (Cheng and Lei, 2001; Sass et al., 2007; Xiang et al., 2015). However, most of the RS-  
76 based retrieval methods make assumptions about the biogeo-optical properties of the  
77 target aquatic system and have spatial-temporal limitations or high demands on the  
78 spectral resolution of RS data, due to the complex optical properties of inland waters  
79 (Shen et al., 2014; Spyros et al., 2018; Ylöstalo et al., 2014). An additional challenge

80 is the calculation of water-leaving reflectance ( $R_{rs}(\lambda)$ ) data globally by removing  
81 various and complex atmospheric effects (Chen et al., 2013a; Wang et al., 2016),  
82 although several atmospheric correction models have been developed to overcome the  
83 atmospheric correction problems for different types of inland waters (Hu et al., 2000;  
84 Shanmugam and Ahn, 2007; Wang and Shi, 2007; Wang et al., 2011; Zhang et al., 2014).  
85 Given these challenges, the development of a globally valid Earth observation approach  
86 for water trophic state assessment has been hindered (Palmer et al., 2015).

87 Here, we promote a water colour index, Forel-Ule index (FUI), as the water quality  
88 parameter to assess trophic state of inland waters. We chose the FUI, which divides  
89 natural waters into 21 colour classes from dark blue to yellowish brown based on the  
90 traditional Forel-Ule scale due to its wide covering of water optical characteristics and  
91 intimate relations with water quality (Wernand and Van der Woerd, 2010; Van der  
92 Woerd et al., 2016). Indeed, water colour expressed through a single colour index is  
93 generally not sufficient to retrieve variables such as Chl-a or suspended sediments  
94 unambiguously (Bukata, 1983; Bukata 1995). However, studies have demonstrated that  
95 water colour is closely associated with the absorption and scattering effects of water  
96 constituents (including Chl-a and suspended sediments), and therefore can be used to  
97 reflect the comprehensive water quality (Garaba et al., 2014; Wang et al., 2015;  
98 Wernand et al., 2013a). Since the FUI can be objectively retrieved using RS  
99 observations at the global scale (Li et al., 2016; Wernand et al., 2013b), it could provide

100 a feasible solution to monitoring global inland water bodies.

101 The main aim of this study was to develop an FUI-based trophic state assessment  
102 approach for global inland waters using the Moderate-resolution Imaging  
103 Spectroradiometer (MODIS) data, and to provide a global-scale view of the water  
104 quality of large lakes and reservoirs worldwide.

## 105 **2. Datasets**

### 106 **2.1 MODIS surface reflectance product**

107 The MODIS level-3 surface reflectance product (MOD09A1) provides data of  
108 mapped surface spectral reflectance at 500 m spatial resolution from 7 bands across the  
109 visible and near infrared and short-wave infrared wavelengths (i.e. 469 , 555, 645, 859,  
110 1240, 1640, and 2130 nm) (Vermote and Vermeulen, 1999). MOD09A1 is an 8-day  
111 composite MODIS Terra product, which is spatially divided by uniform MODIS tiles  
112 on the global scale, which makes it easy to calculate global time-series statistics. It has  
113 been used for long-term and large-area water quality monitoring research as this dataset  
114 is well georeferenced, synthesized, and cloud marked (Hou et al., 2017; Klein et al.,  
115 2017; Li et al., 2016; Wu et al., 2013).

116 In order to retrieve the FUI of global inland waters, we used more than 6400  
117 MOD09A1 images taken during the summer months of 2012 acquired from the  
118 Goddard Space Flight Center (GSFC) of the National Aeronautics and Space  
119 Administration (NASA) (<http://ladsweb.nascom.nasa.gov/index.html>). We chose the

120 year 2012 because of the availability of validation data from published studies and  
 121 online databases about the trophic state of inland waters. Summer months (i.e. from  
 122 June to September in the Northern Hemisphere, and from December to March in the  
 123 Southern Hemisphere) were used to retrieve the FUI, because the biomass of Chl-a-  
 124 containing planktonic algae generally peaks in this season (Singh and Singh, 2015) and  
 125 therefore has the greatest effect on water colour.

## 126 2.2 In-situ dataset

127 Details of the field measured Chl-a and in-situ  $R_{rs}(\lambda)$  are given in in Table 1. The  
 128 in-situ dataset contains 469 samplings from 10 lakes in Asia, North America, and  
 129 Europe. The selection represents different types of inland waters, ranging from a few  
 130 oligotrophic and mesotrophic lakes to more eutrophic lakes, from lakes with high total  
 131 suspended matter (TSM, i.e. Taihu Lake) to lakes with high coloured dissolved organic  
 132 matter (CDOM, i.e. Lake Peipsi and Lake Winnipeg).

133 Table1 Lake Names, locations, number of samplings (N), mean Chl-a concentrations (Chl-a,  $\mu\text{g/L}$ )  
 134 and data sources of the 10 lakes and reservoirs with field measurements

| Lake               | Latitude | Longitude | Chl-a | N   | Data Source                     |
|--------------------|----------|-----------|-------|-----|---------------------------------|
| Lake Maggiore      | 46.01 N  | 8.67 E    | 2.41  | 3   | In-situ (Giardino et al., 2013) |
| Lake Winnipeg      | 51.9 N   | 97.3 W    | 5.33  | 58  | In-situ (Binding et al., 2013)  |
| Lake Erie          | 41.9 N   | 82.1 W    | 9.34  | 24  | In-situ (Binding et al., 2013)  |
| Lake Peipsi        | 58.47 N  | 27.34 E   | 17.95 | 26  | In-situ (Kutser et al. 2013)    |
| Lake Erhai         | 25.86 N  | 100.15 E  | 19.11 | 21  | In-situ                         |
| Yuqiao Reservoir   | 40.04 N  | 117.55 E  | 20.73 | 13  | In-situ                         |
| Guanting Reservoir | 40.35 N  | 115.73 E  | 26.8  | 31  | In-situ                         |
| Taihu Lake         | 31.20 N  | 120.18 E  | 42.6  | 239 | In-situ                         |
| Chaohu Lake        | 31.55 N  | 117.57 E  | 64.47 | 29  | In-situ                         |
| Dianchi Lake       | 24.82 N  | 102.71 E  | 85.2  | 25  | In-situ                         |

135 Equation (1), suggested by Carlson (1977), was applied to the Chl-a dataset:

136 
$$TSI(Chl-a) = 10\left(6 - \frac{2.04 - 0.68 \ln Chl-a}{\ln 2}\right) \quad (1)$$

137 where Chl-a denotes the concentration of Chl-a in  $\mu\text{g/L}$ . The TSI method classifies the  
138 water trophic state as oligotrophic ( $TSI < 30$ ), mesotrophic ( $30 \leq TSI < 50$ ), or eutrophic  
139 ( $TSI \geq 50$ ). The in-situ measured  $R_{rs}(\lambda)$  was used to simulate MODIS bands by using  
140 MODIS spectral response functions (SRF), and then the FUI for these samplings was  
141 calculated to determine the relationship between TSI and FUI.

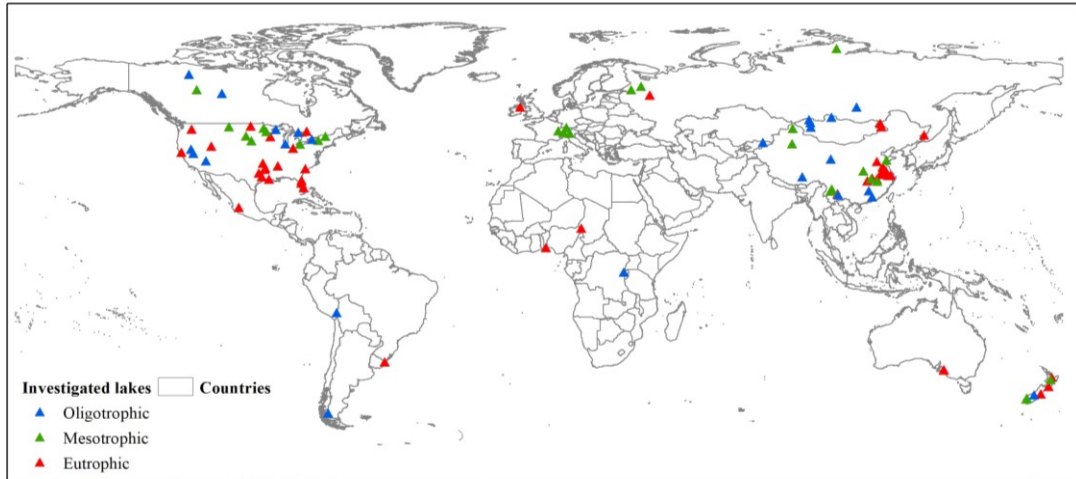
142 Concurrent MOD09 images were acquired to build the data pairs of  $R_{rs}(\lambda)$ . The FUI  
143 was calculated from the data pairs and compared to evaluate the accuracy of MODIS  
144 FUI. The data pairs were coincident within a  $\pm 3$  hour window and the nearest MODIS  
145 image pixel was used to pair with the in-situ data. After removing concurrent MODIS  
146 data with cloud cover, noise cover, and near shoreline pixels, there were 135 pairs of  
147  $R_{rs}(\lambda)$  data from 7 of the 10 lakes. There were 73 pairs for Taihu Lake with 13  
148 concurrent images in July and October 2006, and January and April 2007 (Wang et al.,  
149 2016); 10 pairs for Qinghai Lake with 1 concurrent image in August 2014 (Li et al.,  
150 2016); 10 pairs for Lake Erhai with 1 concurrent image in July 2012; 17 pairs for Lake  
151 Erie (Binding et al., 2013) with 3 concurrent images in August 2012; 20 pairs for Lake  
152 Winnipeg (Binding et al., 2013) with 8 concurrent images in July and August 2012; 4  
153 pairs for Lake Peipsi (Kutser et al., 2013) with 1 concurrent image in June 2012; and 1  
154 pair for Lake Maggiore (Giardino et al., 2013) with 1 concurrent image in July 2012.

155 **2.3 Hydrolight simulated dataset**

156 A Hydrolight simulated Chl-a and  $R_{rs}(\lambda)$  dataset published by (IOCCG, 2006) was  
157 also used to improve the representativeness of oligotrophic to mesotrophic waters in  
158 our dataset, and to illustrate the theoretical relationship between FUI and TSI in these  
159 relatively clear waters. This dataset was simulated using the widely accepted  
160 Hydrolight code (Mobley, 1995), with input inherent optical properties (IOPs)  
161 generated from a wide range of field measurements with various bio-optical models not  
162 limited to Case I water (IOCCG, 2006). The concentration of Chl-a in the simulated  
163 dataset ranges from 0.03 to 30.0  $\mu\text{g/L}$  with an average value of 6.08  $\mu\text{g/L}$ .

#### 164 **2.4 Independent validation dataset**

165 The FUI-based water trophic state assessment results for the summer of 2012 were  
166 validated through comparison with published studies and online databases, including  
167 China Environmental State Bulletin from Ministry of Environmental Protection of the  
168 People's Republic of China (MEPPRC, 2012), and the National Lake Assessment from  
169 the US Environmental Protection Agency (USEPA, 2016). To guarantee objectiveness  
170 and fairness in the validation process, comparison data were only selected where they  
171 represented the whole water body, and where the acquisition time was as close as  
172 possible to the year of 2012. In total, 100 inland water bodies distributed around the  
173 globe were used for validation (Figure 1).



174  
 175  
 176  
 177  
 178  
 179

Figure 1 Spatial distribution and trophic states of 100 water bodies used for validation of the Moderate Resolution Imaging Spectroradiometer (MODIS)-derived Forel-Ule index (FUI) method. Trophic state data were obtained through literature review. Blue triangles denote oligotrophic water bodies, green triangles denote mesotrophic water bodies, and red triangles denote eutrophic water bodies.

### 180 3. Methods

#### 181 3.1 Water-leaving reflectance correction

182 The MODIS surface reflectance products (MOD09) have been corrected for the  
 183 effects of atmospheric gases, aerosols, thin cirrus clouds and adjacency from MODIS  
 184 L1B data (Vermote and Vermeulen, 1999). It was found that the MOD09 reflectance  
 185 was overall greater than the in situ reflectance over inland waters due to the residual  
 186 noises, including the residual aerosol effect, skylight reflection, and possible sun glint  
 187 (Wang, 2016). It is considered that MOD09 often fails to correct for aerosol effect  
 188 because its aerosol input (the MODIS aerosol product, MOD04) usually uses a small  
 189 fill value for the aerosol optical thickness for most inland waters (Wang et al., 2016;  
 190 Vermote and Vermeulen, 1999). In this study, a band subtraction method based on near-

191 infrared (NIR) to short wave infrared (SWIR) bands was used to reduce the noises in  
192 MOD09 data and to convert it to water-leaving reflectance ( $R_{rs}(\lambda)$ ) (Wang, 2016). The  
193 correction equation is:

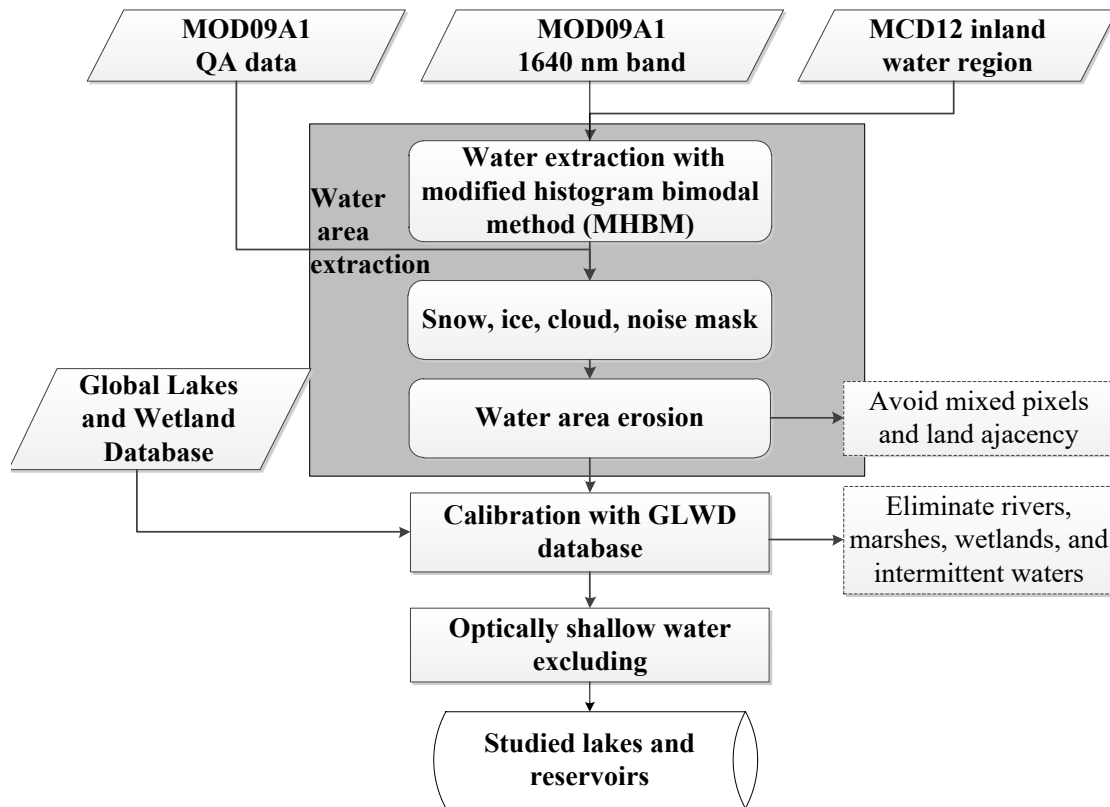
$$194 \quad R_{rs}(\lambda) = \frac{R(\lambda) - \min(R_{NIR} : R_{SWIR})}{\pi} \quad (2)$$

195 where  $R(\lambda)$  is the original reflectance of the MOD09 band, and  $\min(R_{NIR} : R_{SWIR})$  is the  
196 minimum positive value of the NIR and SWIR bands. The  $\min(R_{NIR} : R_{SWIR})$  was  
197 subtracted from each pixel for each band to account for the residual errors (Wang and  
198 Shi, 2007; Wang, 2016). This method neglects the aerosol types, but it can also avoid  
199 the uncertainties in the NIR and SWIR bands being amplified by aerosol exponential  
200 models. The formula is divided by  $\pi$  to convert the surface reflectance to water-leaving  
201 reflectance by neglecting the bidirectional effects. Despite imperfections and  
202 limitations, this method has been shown to achieve accuracies around 30%, and it can  
203 be easily implemented in operational data processing systems for deriving  $R_{rs}(\lambda)$  with  
204 relative stable performances over inland waters under various conditions (Wang et al.,  
205 2016).

### 206 **3.2 Water body identification**

207 The water bodies studied were large lakes and reservoirs (i.e.,  $> 25 \text{ km}^2$  and  
208 covering  $> 100$  pixels in a MOD09A1 image). Water body extraction was taken directly  
209 from satellite data rather than using a static geographic database due to the dynamic  
210 nature of margins of some water bodies. The detection of water pixels in the MOD09A1

211 product was carried out using a series of processing steps on the MODIS satellite data  
 212 outlined in Figure 2.



213  
 214 Figure 2 Flowchart of water body extraction and calibration from MOD09A1 products. MOD09A1  
 215 QA data is the Quality Assurance dataset that included in MOD09A1 dataset. MHBM is the  
 216 modified histogram bimodal method suggested by Zhang et al. (2018).

### 217 3.2.1 Water body extraction and identification

218 The modified histogram bimodal method (MHBM) suggested by Zhang et al.  
 219 (2018) was used to automatically segment water areas from land in the MOD09A1  
 220 image by using the 6<sup>th</sup> band (1640 nm) with a dynamic threshold for each water body.  
 221 The 1640 nm band was selected because it was strongly absorbed by water and strongly  
 222 reflected by terrestrial regions (Mishra and Prasad, 2015). There are six steps in the  
 223 segmentation process as follows:

224 (1) For each water body, the initial water area provided by the MODIS Land Cover  
225 Type product (MCD12Q1 Type-1) (Friedl et al., 2010), which is gridded identically  
226 to MOD09A1, was extended around the coastline reaching a number of 250%  
227 pixels of the water area (including the initial water area).

228 (2) For each water body, a reflectance histogram of the 1640 nm band of the dilated  
229 region was calculated, and the valley value of the histogram falling in the threshold  
230 range was automatically determined as the threshold for the specific water body.  
231 The range of thresholds from a range of representative water types was 0.005 to  
232 0.11;

233 (3) Water bodies were segmented from MOD09A1 images using the determined  
234 thresholds;

235 (4) MOD09A1 Quality Assurance (QA) data (Vermote et al., 2015) were used to  
236 eliminate cloud, ice, and snow cover, and low quality pixels from the water areas;

237 (5) Extracted water areas were eroded with a 500 m buffer to avoid the effects of mixed  
238 land-water pixels and severe land adjacency near the shoreline and to ensure the  
239 quality of water pixels (Hou et al., 2017);

240 (6) Water bodies with areas of water connected with more than 100 pixels (i.e., > 25  
241 km<sup>2</sup>) were selected for this study.

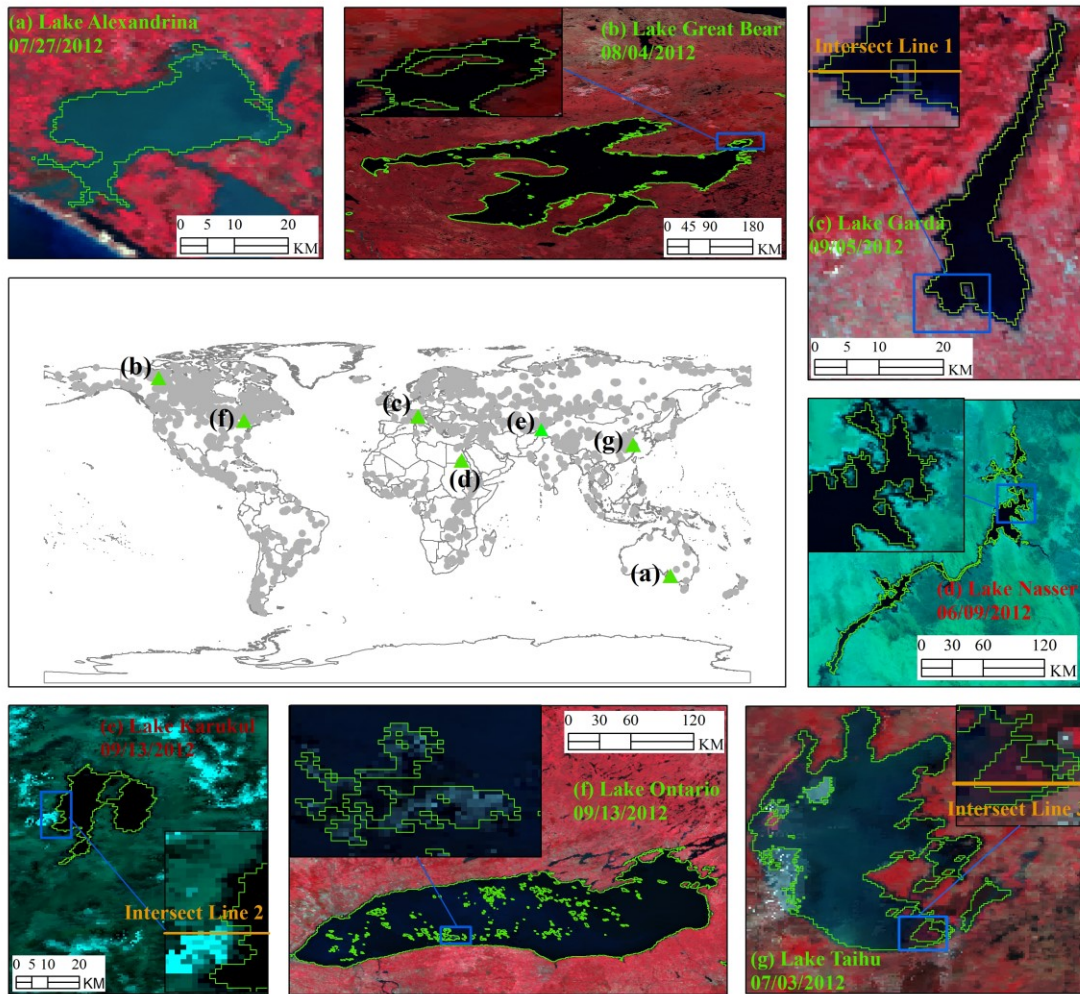
242 The 500 m buffer was determined according to the comparison of MODIS  $R_{rs}(\lambda)$   
243 in the transects selected from the land–water boundaries; it showed that generally, one

244 pixel (500 m) near the shoreline at the visible bands was subject to detectable adjacency  
245 contamination, which is consistent with the findings of Hou et al. (2017). Notably, the  
246 land adjacency effect for MODIS may theoretically have an impact at much larger  
247 distances offshore (Bulgarelli and Zibordi, 2018), but considering that the uncertainty  
248 in MODIS  $R_{rs}(\lambda)$  is already approximately 30%, the adjacency effect at distances greater  
249 than 500 m may not be obvious.

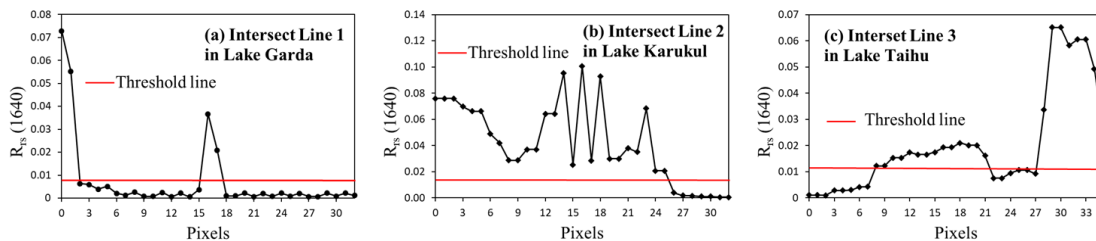
250 Figure 3 shows the examples of water segmentation from MOD09A1 data. It  
251 demonstrates that the water pixels have characteristically low reflectance values which  
252 aids in detection against different land cover types, including small islands (Figure 3 (b)  
253 and (c)), clouds (Figure 3 (f) and (g)), snow and ice (Figure 3 (e)), aquatic plants (Figure  
254 3 (g)) and low quality pixels (Figure 3 (g)). The  $R_{rs}(1640)$  values of the intersect lines  
255 (marked in Figure 3) under different conditions are shown in Figure 4.

256 The extracted water areas were intersected with the Global Lakes and Wetland  
257 Database (GLWD) (Lehner and Döll, 2004), which represents a compilation of  
258 numerous existing maps and datasets and has been validated comprehensively for lakes >  
259 1 km<sup>2</sup>. GLWD Level 3 (GLWD-3) comprises lakes, reservoirs, rivers and different  
260 wetland types in the form of a global raster map at 30-second resolution. Since the aim  
261 of this study is to assess the trophic state of lakes and reservoirs at the global scale,  
262 water bodies with centroid points located in the lake or reservoir type in the GLWD-3  
263 database were chosen, and those located in rivers, ephemeral waters, coastal wetland

264 and other types of wetland were removed.



265  
 266 Figure 3 Shorelines of water bodies extracted from MOD09A1 images using the modified histogram  
 267 bimodal method (MHBM). (a) Lake Alexandrina in Australia; (b) Lake Great Bear in North America;  
 268 (c) Lake Garda in Europe; (d) Lake Nasser in Africa; (e) Lake Karukul in Asia; (f) Lake Ontario in  
 269 North America; (g) Lake Taihu in Asia. Green lines denote shorelines. Backgrounds are standard  
 270 false colour images where red, green, and blue are the 859 nm, 645 nm and 555 nm bands of the  
 271 MOD09A1 image, respectively. The image acquisition date is listed in each subfigure. The  $R_{rs}(1640)$   
 272 values of the three intersect lines are shown in Figure 4.



273  
 274 Figure 4 The  $R_{rs}(1640)$  values of the intersect lines that marked in Figure 3. (a) Intersect Line 1

275 through Lake Garda crosses an island inside the lake; (b) Intersect Line 2 through Lake Karukul  
276 crosses snow covering the shore side; (c) Intersect Line 3 through Lake Taihu crosses obvious  
277 aquatic plants in the water.

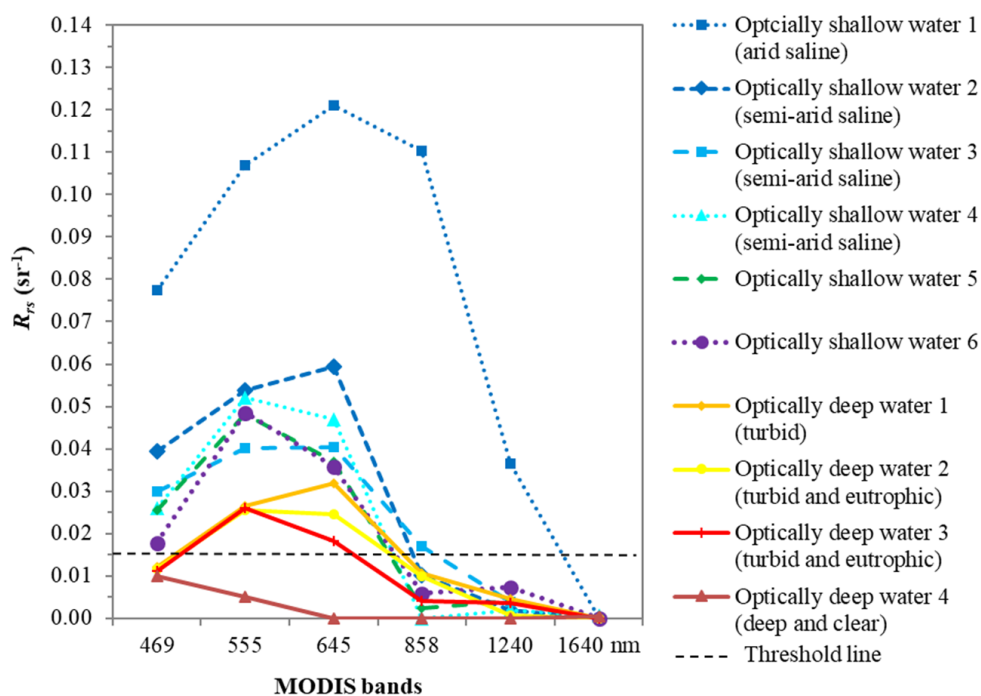
### 278 **3.2.2 Excluding optically shallow water**

279 The extracted water pixels were tested for optically shallow water. Even though  
280 optically shallow water for large inland waters ( $>25 \text{ km}^2$ ) is seldom found once the  
281 identified wetlands in GLWD database are removed, it is possible that bottom  
282 reflectance may influence observed water colour, for example in arid or semi-arid saline  
283 lakes. Numerous radiative transfer models have been developed that account for the  
284 effects of the bottom reflectance and water column on remotely sensed  $R_{rs}(\lambda)$  (Lyzenga,  
285 1978; Philpot, 1989; Maritorena et al., 1994; Lee et al., 1998; Mobley and Sundman,  
286 2003). The response types of  $R_{rs}(\lambda)$  spectral curves differ with changes in bottom status,  
287 water depth, and optical properties of the water (Holden and LeDrew, 2002; Ma et al.,  
288 2014; Lee et al., 1998; Lim et al., 2009), and there is no single method that can  
289 accurately detect optically shallow water in lakes at the global scale.

290 To address these challenges, a three-stage method combining automatic  
291 identification with manual-intervention was used to identify the optically shallow water  
292 bodies:

293 (1) The MODIS SWIR band (1640 nm) threshold method was adopted in water area  
294 segmentation, so that shallow waters with benthic aquatic plants were eliminated  
295 from water area due to the higher reflectance in the SWIR band from the aquatic  
296 plant that would not be presented in deeper waters (Li et al., 2009);

297 (2) The blue band threshold method was used as a preliminary means for identifying  
 298 shallow waters containing a signal from highly reflective sand and sediment  
 299 bottoms (Lim et al., 2009; Mobley and Sundman, 2003). The threshold ( $R_{rs}(469$   
 300  $\text{nm}) = 0.015 \text{ sr}^{-1}$ ) was determined by collecting and comparing a large number of  
 301  $R_{rs}(\lambda)$  spectra of optically shallow and deep waters derived from MOD09A1  
 302 images in the summer of 2012 (Figure 5);  
 303 (3) Shallow water bodies identified in the first two steps were reviewed using Google  
 304 Earth and relevant publications (Williams, 2002; Hurlbert, 2012), to remove lakes  
 305 and reservoirs characterized by deep waters.



306  
 307 Figure 5 Typical water-leaving reflectance ( $R_{rs}(\lambda)$ ) spectra of optically shallow waters and optically  
 308 deep waters derived from MOD09A1 images in the summer of 2012. The optically shallow waters  
 309 1-4 are Lake Beihuo Luxun, Lake Manas, Lake Margai Caka, and Lake Gasi Kule from Northwest  
 310 China, and they were described as arid and semi-arid saline lakes in Wang and Dou (1998). The  
 311 identified optically shallow waters 5 and 6 are Lake George in Australia (Fitzsimmons and Barrows,  
 312 2010) and shallow water near the island bank in the Bahamas, respectively (Dierssen et al., 2003);

313 The dotted line denotes the threshold line ( $0.015 \text{ sr}^{-1}$ ) of  $R_{rs}(469 \text{ nm})$  that used to separate the  
314 optically shallow waters.

### 315 **3.3 FUI retrieval method**

316 In the Commission on Illumination (CIE) colourimetry system, theoretically colour  
317 parameters can be calculated from hyperspectral  $R_{rs}(\lambda)$  and colour-match functions by  
318 using spectral integration in the visible range (C.I.E., 1932; Wang et al., 2015). As there  
319 are only three red, green, blue (RGB) bands in MOD09 images (645 nm, 555 nm and  
320 469 nm), the RGB conversion method was used to calculate CIE X, Y, Z using the  $R_{rs}(\lambda)$   
321 at the three visible bands (Wang et al., 2015; Li et al., 2016). The RGB conversion  
322 equation to X, Y, Z is as follows:

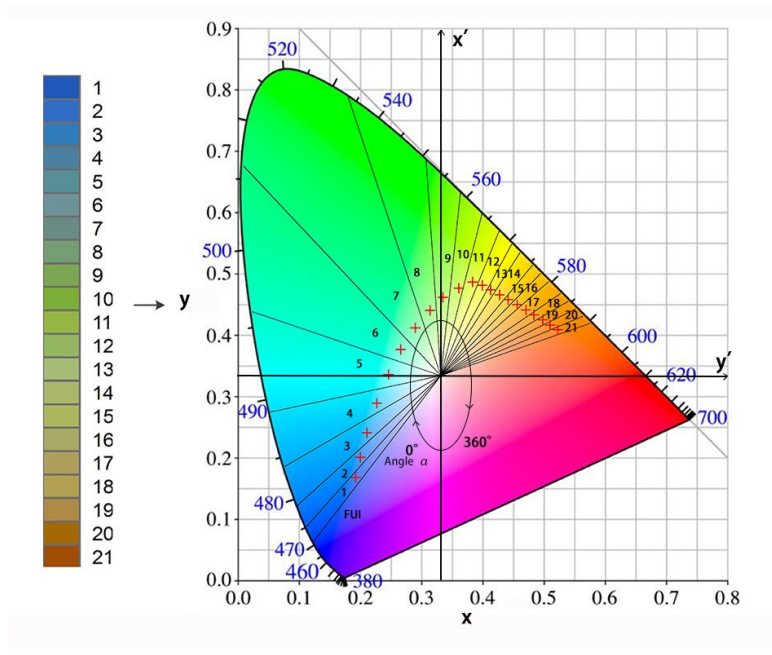
$$\begin{aligned} 323 \quad X &= 2.7689R + 1.7517G + 1.1302B \\ 324 \quad Y &= 1.0000R + 4.5707G + 0.0601B \\ 325 \quad Z &= 0.0000R + 0.0565G + 5.5934B \end{aligned} \quad (3)$$

326 CIE chromaticity coordinates ( $x, y$ ) were then calculated from the X, Y, Z by  
327 normalizing them to between 0 and 1. A new coordinate system ( $x', y'$ ) was built based  
328 on the chromaticity coordinates ( $x, y$ ) as (Figure 6):

$$\begin{aligned} 329 \quad x' &= y - \frac{1}{3} \\ 331 \quad y' &= x - \frac{1}{3} \end{aligned} \quad (4)$$

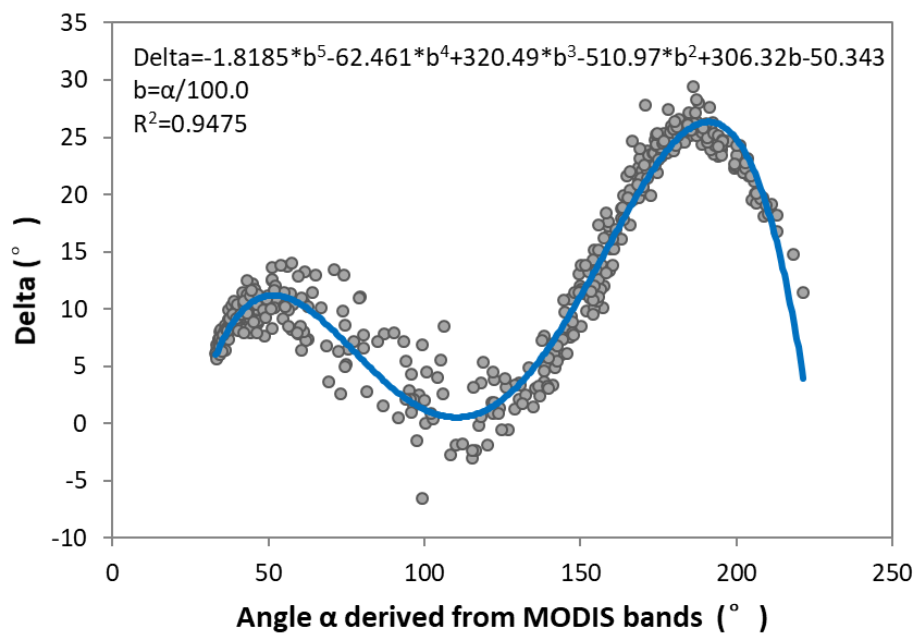
332 Based on the coordinates ( $x', y'$ ) in the CIE chromaticity diagram, angle  $\alpha$  was  
333 calculated, defined as the angle between the vector of coordinates ( $x', y'$ ) and the

334 negative  $x'$ -axis (at  $y = 1/3$ ) in the new coordinate system. It is notable that angle  $\alpha$  is  
335 basically consistent with the definition reported in Wang et al. (2015); but for the  
336 convenience of subsequent calculation, starting from the negative  $x'$ -axis, the angle  $\alpha$   
337 is improved to remain positive now from  $0^\circ$  to  $360^\circ$ . Due to the band setting of satellite  
338 sensors, there is a difference between the human eye sensed true colour and the sensor  
339 derived colour (Van der Woerd and Wernand, 2015). To eliminate the colour difference  
340 caused by MODIS band setting, a systematic deviation delta, defined as the difference  
341 between angle  $\alpha$  derived from hyperspectral  $R_{rs}(\lambda)$  and the equivalent MODIS bands,  
342 was modelled and calculated. Following the method presented in Van der Woerd and  
343 Wernand (2015), the delta for MODIS was modelled with a polynomial fitting (Figure  
344 7) based on the simulated dataset generated by Hydrolight (IOCCG, 2006). With this  
345 delta correction, the angle  $\alpha$  and the FUI can be transferable between satellites and  
346 sensors with different spectral settings (Van der Woerd and Wernand, 2015). Finally,  
347 based on angle  $\alpha$  after delta correction, the FUI was calculated using the 21-class FUI  
348 lookup table established from the chromaticity coordinates of the Forel-Ule scales  
349 (Novoa et al., 2013, Figure 6).



350

351 Figure 6 The FUI colours and the subdivision of the FUI from 1 to 21 in the CIE chromaticity  
 352 diagram. The red crosses mark the chromaticity coordinates of the Forel-Ule scales (Novoa et al.,  
 353 2013). Angle  $\alpha$  is the angle between the vector to a point and the negative  $x'$ -axis (at  $y = 1/3$ ).



354

355 Figure 7 Deviation delta ( $^{\circ}$ ) from the hyperspectral angle  $\alpha$  as a function of MODIS derived angle  
 356  $\alpha$  for  $0^{\circ} < \alpha < 230^{\circ}$  (i.e., FUI ranging from 1 to 20)

### 357 3.4 FUI-based trophic state assessment algorithm

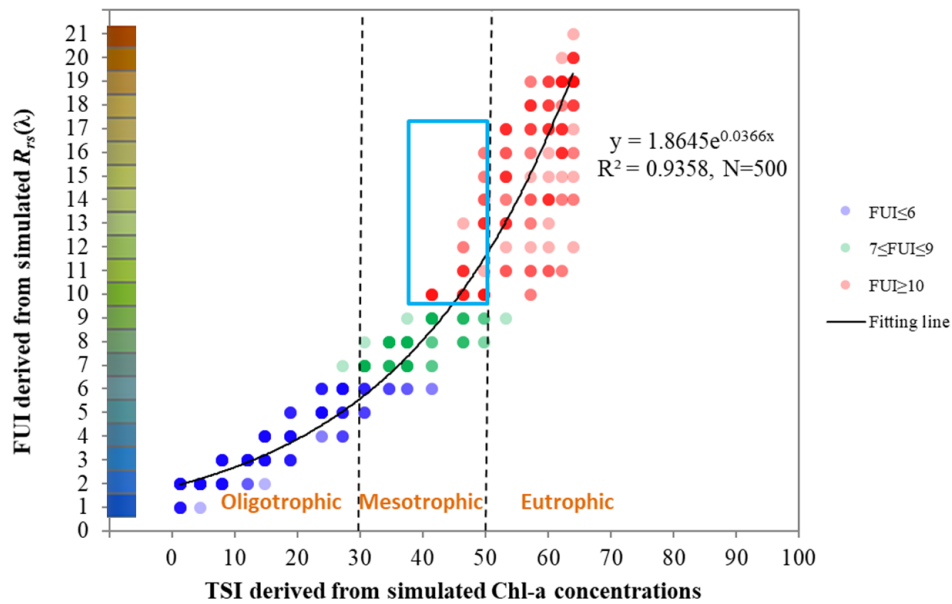
358 Calculations of the FUI and TSI were initially derived from the Hydrolight

359 simulated dataset to build the theoretical relationship between the two quantities in  
360 relatively clear Chl-a dominated waters (Figure 8). Values for TSI ranged from 0 to 68,  
361 the FUI generally increased with TSI based on the simulated dataset ( $R^2 = 0.94$ ,  $N =$   
362 500).

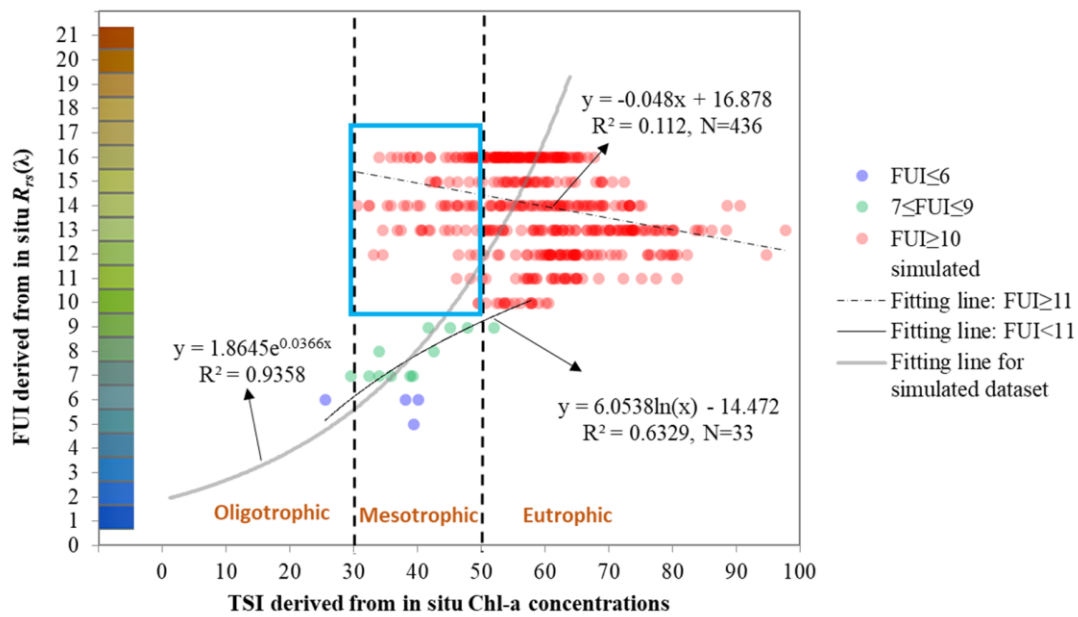
363 However, the relationship between FUI and TSI from the in-situ dataset (Table 1)  
364 showed a unimodal distribution (Figure 9): (i) similar to the simulated dataset, when  
365  $FUI < 10$ , it increased with TSI ( $R^2 = 0.633$ ), showing that when water colour changes  
366 from blue to green, the water body changes from oligotrophic to mesotrophic; (ii) TSI  
367 peaked when FUI approached 10, because highly eutrophic waters generally appear  
368 green owing to high Chl-a content; (iii) when  $FUI > 10$ , it showed a scattered negative  
369 relationship with TSI ( $R^2 = 0.112$ ), reflecting the shift from green to brown associated  
370 with turbid eutrophic, or humic waters. Based on the in-situ dataset, the relationship for  
371  $FUI > 10$  is scattered and loose (Figure 9) because of complex constituents varying  
372 independently in turbid waters, but this occasion is underrepresented in the simulated  
373 dataset in Figure 8.

374 Although there are insufficient oligotrophic and mesotrophic waters in the in-situ  
375 dataset, the in-situ dataset in Figure 9 showed a roughly similar overall trend as the  
376 simulated dataset in Figure 8, and presented the FUI ranges for different trophic states.  
377 The dataset showed that 82.7% of in-situ data points with FUI values  $\geq 10$  were  
378 eutrophic with  $TSI \geq 50$ ; 83.3% of points with  $7 \leq FUI < 10$  (i.e., 10 points out of 12)

379 were mesotrophic while the other two points had TSI values of 29.5 and 50.5. Finally,  
 380 data points with  $FUI < 7$ , were classified as oligotrophic, which is supported by the  
 381 simulated dataset. The FUI ranges were consequently used to classify the trophic state  
 382 of the waters.



383  
 384 Figure 8 Scatterplot of data pairs of the Forel-Ule index (FUI) and Chl-a-based trophic state index  
 385 (TSI) from the Hydrolight simulated dataset (N = 500) (IOCCG, 2006). The colour bar indicates the  
 386 colour of the FUI indices. This simulated dataset covers a wide range of natural waters with  
 387 concentrations of Chl-a from 0.03 to 30.0  $\mu\text{g/L}$ . The points were plotted with 60% transparency to  
 388 show the data density. The cyan box marks the mesotrophic points with  $FUI \geq 10$ .



389

390 Figure 9 Scatterplot of data pairs of the Forel-Ule index (FUI) and concurrent Chl-a-based trophic  
 391 state index (TSI) from in-situ measurements (N = 469). The colour bar indicates the colour of the  
 392 FUI indices. Blue points denote  $FUI \leq 6$ , green spots denote  $7 \leq FUI \leq 9$ , and red spots denote  $FUI$   
 393  $\geq 10$ . The spots were plotted with 60% transparency to show the density of observations. The cyan  
 394 box marks the mesotrophic points with  $FUI \geq 10$ .

395 Some humic (i.e., high CDOM content) or turbid (i.e., high TSM content)

396 mesotrophic waters may result in an FUI value greater than 10 with green to brown

397 colour, such as the scattered points presented in the cyan box in Figure 8 and Figure 9.

398 To distinguish these points, a red band ( $R_{rs}(645)$ ) threshold method was implemented

399 by comparing the  $R_{rs}(\lambda)$  spectra of these points with representative  $R_{rs}(\lambda)$  spectra of

400 eutrophic waters. Even if water bodies with high CDOM but low TSM appear with a

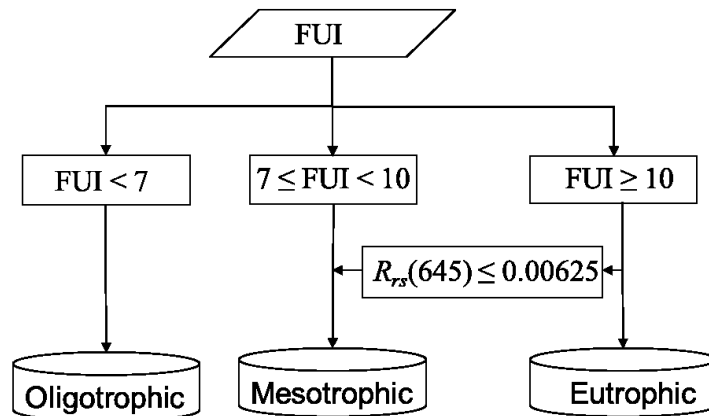
401 high colour index,  $R_{rs}(645)$  will be relatively low compared with other TSM-dominated

402 yellow waters due to low backscattering of the water constituents with high CDOM and

403 low TSM. After applying this threshold, the accuracy of eutrophic classification was

404 increased to 86.8%. With the FUI subsection and the  $R_{rs}(645)$  threshold, a decision tree

405 of trophic state assessment for water bodies was developed, shown in Figure 10.  
 406



407  
 408 Figure 10 Forel-Ule index (FUI)-based water trophic state assessment decision tree based on the  
 409 classification of FUI and  $R_{rs}(645)$

410 Lake-average values were considered more appropriate for global applications of  
 411 the method. Results showed a positive relationship between lake-average FUI and lake-  
 412 average TSI. For the 10 lakes sampled during 14 field campaigns, only 1 pair of  
 413 FUI/TSI averages was misclassified based on the FUI from the 10-lake in-situ dataset,  
 414 supporting the applicability of the method to lake averages.

### 415 3.5 Spatial and Temporal statistics

416 As MOD09A1 is an 8-day composite product, there are globally 16 periods of  
 417 MOD09A1 images over the four summer months. The seasonal average FUI for each  
 418 study lake was estimated and used to assess the trophic state of lakes in the summer of  
 419 2012. During the calculation, a standard water mask image was produced for each lake  
 420 by overlaying the water mask images in the same MODIS tile. This was used to check  
 421 the percentage of noise pixels covered by clouds, ice, snow, and other noises. If the  
 422 detected water pixels for a lake in an image was less than 30% of its standard water

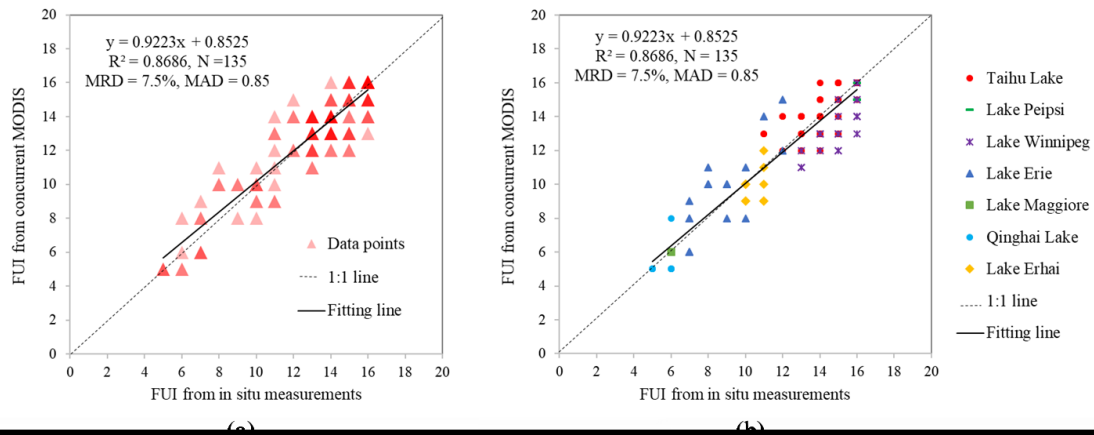
423 mask area, then those pixels were not considered to represent the entire lake and the  
424 image was not used for lake assessment. If less than 3 of the 16 images were valid for  
425 a lake over the summer months, then the lake was not assessed in this study. A water  
426 body spanning more than one tile of the MOD09A1 image was merged into a single  
427 lake by detecting the connected area in the standard water mask images across tiles. To  
428 show the variations within each lake, the spatial coefficient of variation ( $CV = \delta/\mu$ ,  
429 where  $\delta$  is the standard deviation and  $\mu$  is the mean) of the FUI and the temporal  
430 coefficient of variation for each study lake was also calculated. The average  $R_{rs}(645)$   
431 for each lake was computed to aid the FUI-based trophic state assessment.

## 432 **4. Results**

### 433 **4.1 Evaluation of MODIS retrieved FUI**

434 The FUI values derived from MOD09  $R_{rs}(\lambda)$  and concurrent in-situ  $R_{rs}(\lambda)$  were  
435 compared to evaluate the FUI retrieved from MODIS with the water-leaving reflectance  
436 correction. Despite a few scattered points (with light red colour in Figure 11(a)) that  
437 may be caused by the complex atmospheric conditions (e.g. land aerosols), the paired  
438 data from the seven lakes showed a strong correlation that mostly fell along the  
439 approximate 1:1 line (Figure 11;  $R^2 = 0.87$ , slope = 0.92), with a mean absolute  
440 difference (MAD) of 0.85 and a mean relative difference (MRD) of 7.5%. In addition,  
441 the MODIS FUI produced a 10.5% difference in trophic state classification, compared  
442 with the FUI derived from in-situ  $R_{rs}(\lambda)$ . The effects of various aerosol and

443 solar/viewing geometry perturbations on the FUI calculation are discussed in Section  
444 5.1.



445  
446 Figure 11 Scatterplots of the FUI derived from in-situ measured  $R_{rs}(\lambda)$  versus concurrent MOD09  
447 retrieved  $R_{rs}(\lambda)$  for seven lakes with different FUI ranges. (a) Data points are coloured with 60%  
448 transparency; darker spots indicate a higher data density. (b) Data points from different lakes are  
449 marked with different symbols.

#### 450 4.2 Validation results with independent data

451 The lake trophic state data included in the independent validation dataset, as well  
452 as the sources of the trophic states data, are listed in Table S1 in Supplementary Material.  
453 We found that 20 of the 100 water bodies were misclassified using the FUI-based  
454 method. There were no misclassifications between eutrophic and oligotrophic water  
455 bodies. Most misclassifications occurred between eutrophic and mesotrophic water  
456 bodies, and to a lesser extent between mesotrophic and oligotrophic water bodies. The  
457 user accuracy of the oligotrophic, mesotrophic, and eutrophic classifications was  
458 100.0%, 66.7%, and 78.3%, respectively, calculated through confusion matrix analysis.  
459 The overall accuracy of the trophic state assessment was found to be 80.0% ( $R^2 = 0.75$ ),  
460 while the Kappa coefficient (Landis and Koch, 1977) was 0.67 (Table 2), which

461 confirmed that the FUI-based results were substantially consistent with the comparison  
 462 dataset.

463 Table 2 Confusion matrix of Forel-Ule index (FUI)-based trophic state assessment for the  
 464 investigated 100 lakes

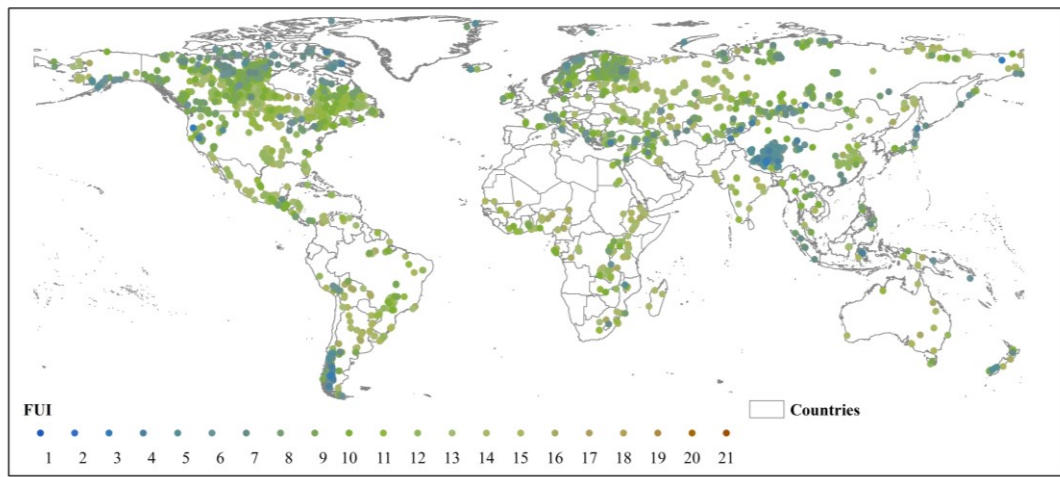
| Comparison<br>FUI-based<br>Assessment \ Data | Oligotrophic | Mesotrophic | Eutrophic | Total | User accuracy |
|--|--------------|-------------|-----------|-------|---------------|
| Oligotrophic                                 | 19           | 0           | 0         | 19    | 100.0%        |
| Mesotrophic                                  | 5            | 14          | 2         | 21    | 66.7%         |
| Eutrophic                                    | 0            | 13          | 47        | 63    | 78.3%         |
| Total  | 24           | 27          | 49        | 100   |               |
| Producer accuracy                            | 79.2%        | 51.9%       | 95.5%     |       |               |
| Kappa coefficient                            | 0.67         |             |           |       |               |
| Overall accuracy                             | 80.0%        |             |           |       |               |

465

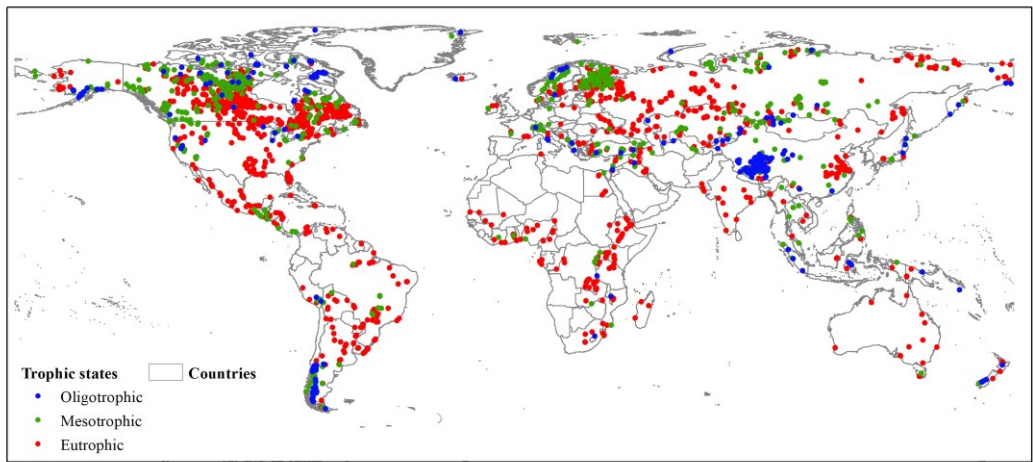
### 466 4.3 Trophic state assessment for global inland waters in 2012

467 Among the water bodies studied (N = 2058, total surface area = 1.73 million km<sup>2</sup>),  
 468 the MODIS FUI of the lakes in the summer of 2012 ranged from 2.0 to 17.0, the spatial  
 469 CV of the water bodies ranged from 0.0% to 41.2% with an average value of 12.9%  
 470 and the temporal CV ranged from 0.0% to 54.3% with an average value of 9.9%. The  
 471 season-averaged FUI values of the studied large lakes were found to vary between 3.1  
 472 and 16.0, and the mean FUI was 11.1 with a worldwide CV of 26.6% (Figure 12). Based  
 473 on these data, the results presented that large lake trophic states were not equally  
 474 distributed around the globe, shown in Figure 13. Eutrophic water bodies accounted for  
 475 63.1% of the total number but only 30.5% of the total surface area, mesotrophic water  
 476 bodies accounted for 26.2% of the total number and 39.4% of the total surface area, and

477 oligotrophic water bodies accounted for 10.7% of the total number but 30.1% of the  
478 total surface area.



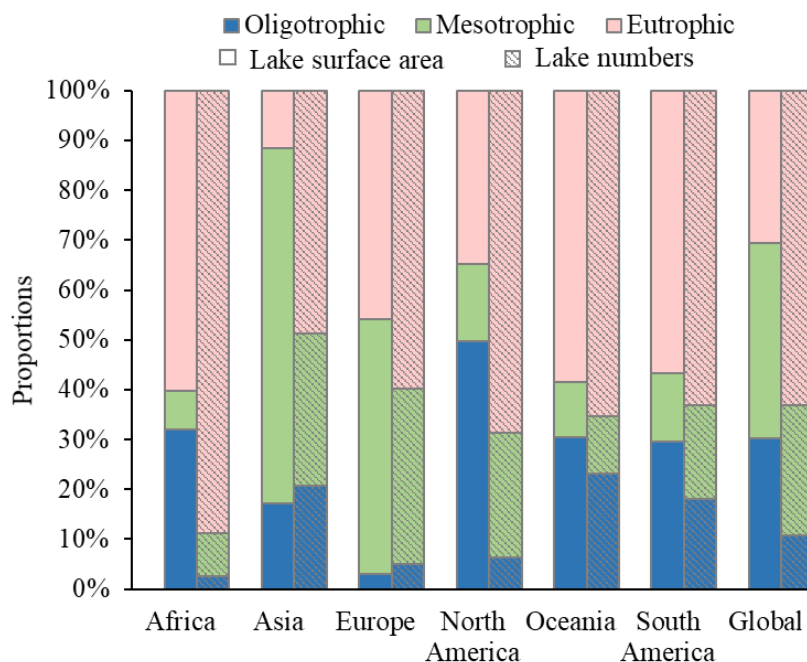
479  
480 Figure 12 MODIS FUI values for global inland waters in the austral and boreal summers of 2012.  
481 Each point represents a single water body of > 25 km<sup>2</sup> in surface area. The FUI of each point  
482 represents averaged values from all lake pixels across the summer months rounded to the nearest  
483 integer.



484  
485 Figure 13 Trophic state classification of global inland waters in the austral and boreal summers of  
486 2012 assessed using the FUI-based method. Blue spots denote oligotrophic water bodies, green spots  
487 denote mesotrophic water bodies, and red spots denote eutrophic water bodies.

488 It was found that oligotrophic large lakes concentrated in high mountains and  
489 plateau regions of Central Asia (Qinghai-Tibet Plateau region) and southern South  
490 America (Patagonia Plateau region), while eutrophic large lakes concentrated in central

491 Africa, eastern Asia (East China), and mid-northern and southeast North America  
 492 (south Canada and southeast U.S.). In terms of lake numbers, Oceania had the highest  
 493 proportion of oligotrophic large lakes (23.1%), Europe had the highest proportion of  
 494 mesotrophic large lakes (35.2%), and Africa had the highest proportion of eutrophic  
 495 large lakes (88.8%). In terms of surface area, North America had the highest proportion  
 496 of oligotrophic water (49.8%), Asia had the highest proportion of mesotrophic water  
 497 (71.2%), and Africa still had the highest proportion of eutrophic water (Figure 14).

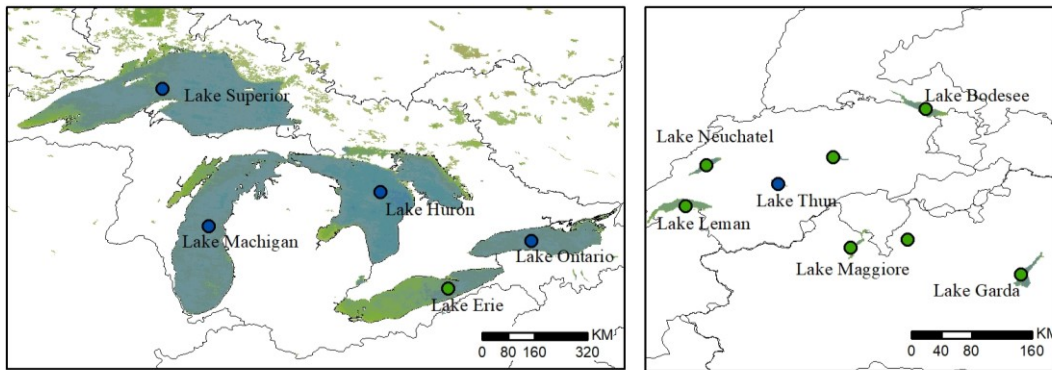


498  
 499 Figure 14 Proportion of large lakes with each trophic state in terms of lake number and lake  
 500 surface area across continents.

501 **4.4 Trophic state assessment for regional groups of lakes**

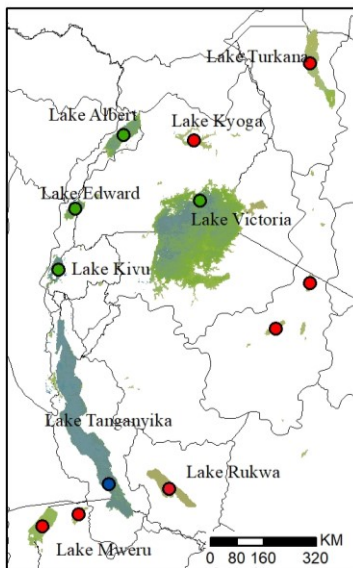
502 To further validate the FUI-based trophic state results, data from five regional  
 503 groups of lakes around the world were analyzed (Figure 15): the North America Great  
 504 Lakes region (oligo-mesotrophic dominated), the African Great Lakes region

505 (mesotrophic dominated), the central south European region (mesotrophic dominated),  
 506 the east Asian middle-lower Yangtze region (eutrophic dominated), and the Tibet  
 507 Plateau (oligotrophic dominated).

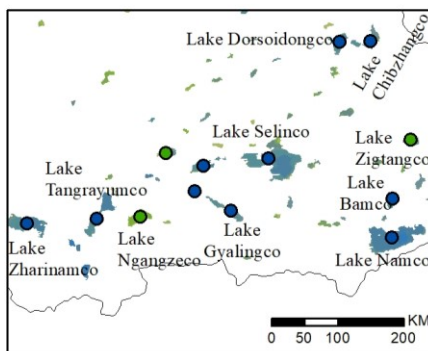
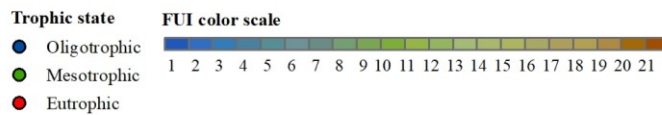
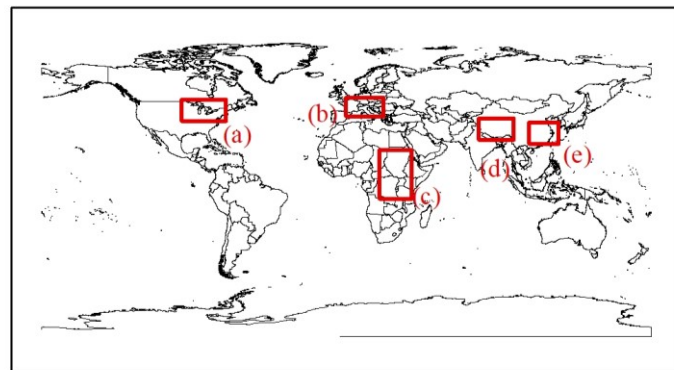


(a)

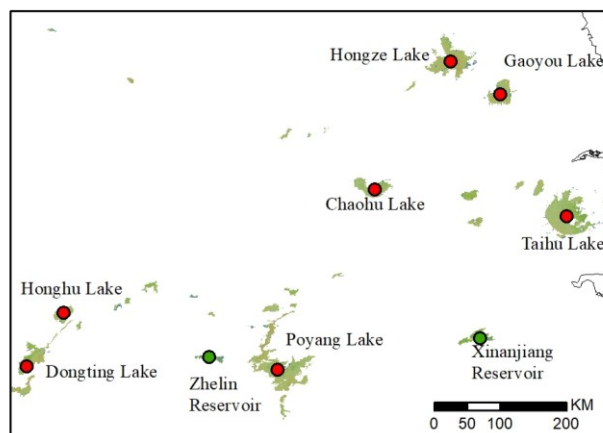
(b)



(c)



(d)



(e)

508

509 Figure 15 Trophic states and Forel-Ule index (FUI) values of large lakes within typical lake regions  
510 in the austral and boreal summers of 2012: (a) North America Great Lakes region; (b) central south  
511 European; (c) African Great Lakes region; (d) Tibet Plateau; (e) middle-lower Yangtze region.  
512 Coloured points represent the mean trophic state of the water body (blue spots denote oligotrophic  
513 water bodies, green spots denote mesotrophic water bodies, and red spots denote eutrophic water  
514 bodies).

515

516 The FUI of lakes in the North America Great Lakes region mainly ranged from 5  
517 to 10, corresponding to a cyan water colour. Lake Superior, Lake Michigan, Lake  
518 Ontario and Lake Huron were found to be oligotrophic, while Lake Erie was found to  
519 be mesotrophic. The water colour of western Lake Erie is greener than the other lakes  
520 and had an FUI of ~11 (i.e., eutrophic). These results are consistent with those of past  
521 studies (Auer et al., 2004; Barbiero et al., 2012; Bridgeman et al., 2013; Chaffin et al.,  
522 2011; Holeck et al., 2015; Mukherjee et al., 2016; Shuchman, 2013).

523 The FUI of lakes in the central south European region mainly ranged from 7 to 9,  
524 corresponding to a cyan water colour and a mesotrophic state. This is consistent with  
525 past studies, which have classified water bodies in this region as oligo-mesotrophic  
526 (Coci, et al., 2015; Rimet et al., 2015; Fuentes et al., 2013; Giardino et al., 2014; Jaquet,  
527 2013; Stich and Brinker, 2010; Vollenweider and Kerekes, 1982).

528 The FUI of lakes in the African Great Lakes region, which constitutes part of the  
529 Rift Valley and East African Rift, mainly varied from 4 to 16, corresponding to a water  
530 colour of cyan to green and a wide range of trophic states (oligotrophic, mesotrophic,  
531 and eutrophic). Lake Victoria, the second largest freshwater lake in the world, is

532 mesotrophic with eutrophic sections. Lake Turkana, one of the largest desert lakes in  
533 the world and the most important regional source of fish, is eutrophic. Lake Tanganyika,  
534 the deepest lake in Africa, is oligotrophic. These results are consistent with the past  
535 studies (Hecky et al., 2010; Okullo et al., 2011; Avery, 2012; Velpuri et al., 2012;  
536 O'Reilly, 2003; Verburg, 2006).

537 The FUI of lakes on the Tibet Plateau ranged from 2 to 7, corresponding to a water  
538 colour of blue to cyan and trophic states that are mainly oligotrophic. Lake Namco,  
539 which lies at an elevation of 4718 m and experiences low impact from human activity  
540 (Wang and Dou, 1998), was shown to have a very low FUI (2–4) and be oligotrophic.  
541 Compared with Lake Namco, the FUI of Lake Selinco was higher (4–7), and its trophic  
542 state was oligotrophic but approaching mesotrophic (Li et al., 2016). The FUI of Lake  
543 Ngangzeco and Lake Zigtangco were found to be even higher and their trophic states  
544 were mesotrophic. Few studies have been implemented for the water trophic states on  
545 the Tibet Plateau due to the poor weather conditions. The results in Figure 15 (d) can  
546 fill the knowledge gap in this region.

547 The FUI of the lakes in the middle-lower Yangtze region mainly ranged from 9 to  
548 14, corresponding to a water colour of green to yellow-green, and the trophic states  
549 were mainly eutrophic. This is consistent with past studies, which have demonstrated  
550 that Lake Taihu, Lake Chaohu, Lake Poyang, and Lake Dongting are typical eutrophic  
551 and turbid lakes in China (Chen et al., 2013a, 2013b; Shi et al., 2015; Wang et al., 2011;

552 Wu et al., 2013; Yang et al., 2013). The trophic states of the Xin'anjiang and Zhelin  
553 reservoirs, the two largest reservoirs on the middle-lower reach of the Yangtze, were  
554 found to be mesotrophic, which agrees with the results of published literature (Chen,  
555 2009; Sheng et al., 2015).

## 556 **5. Discussion**

### 557 **5.1 FUI sensitivity to aerosol perturbations and observation conditions**

558 The significant positive correlation between the concurrent FUIs over a wide range  
559 of lakes, and the relatively low uncertainties suggest that MODIS surface reflectance  
560 data and the water-leaving correction method can be used for FUI retrieval and the FUI-  
561 based trophic state assessment of water bodies. Moreover, it is notable that in  
562 comparison with concurrent in-situ data (Figure 11), the accuracy of the MODIS FUI  
563 (~90%) was greater than that of MODIS  $R_{rs}(\lambda)$  (Wang et al., 2016), indicating that the  
564 FUI calculation process can reduce uncertainties introduced in MODIS  $R_{rs}(\lambda)$ .

565 However, the MOD09  $R_{rs}(\lambda)$  retrieved still theoretically contains some of the  
566 uncertainties induced by the effects of aerosol types and bidirectional properties as a  
567 result of the MOD09 data and the water-leaving correction method. Hence, the  
568 sensitivities of FUI to these uncertainties within the input data were investigated using  
569 radiative transfer model simulations. These simulations verified the general global  
570 applicability of FUI calculated with this method.

571 Based on the radiative transfer theory and assuming a non-coupling water-

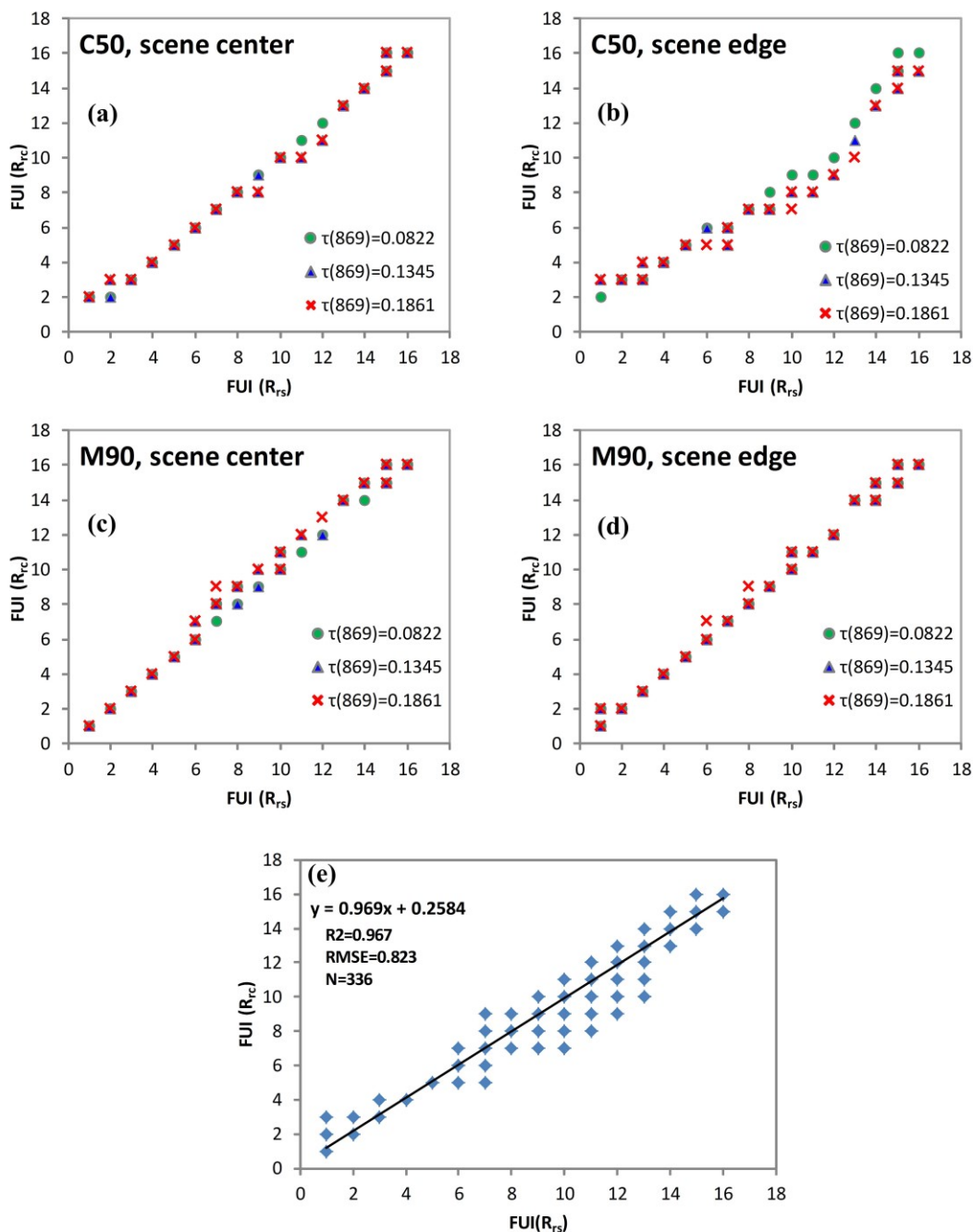
572 atmosphere system, Rayleigh-corrected reflectance ( $R_{rc}$ ) can be expressed as:

$$573 \quad R_{rc}(\lambda) = \rho_t(\lambda) - \rho_r(\lambda) = \rho_a(\lambda) + \pi t(\lambda)t_0(\lambda)R_{rs}(\lambda) \quad (5)$$

574 where  $\rho_t(\lambda)$  is the top-of atmosphere (TOA) reflectance,  $\rho_r(\lambda)$  is the reflectance due to  
575 Rayleigh scattering,  $\rho_a(\lambda)$  is the aerosol reflectance including that from aerosol  
576 scattering and aerosol-Rayleigh interactions,  $t(\lambda)$  is the atmospheric transmittance from  
577 the target to the satellite sensor, and  $t_0(\lambda)$  is the atmospheric transmittance from the Sun  
578 to the target. These unknowns can be calculated from SeaDAS LUTs (look-up tables)  
579 for variable aerosols and solar/viewing geometry. Thus, the relationship between  $R_{rs}(\lambda)$   
580 and the  $R_{rc}(\lambda)$  containing various aerosols can be established through simulations. To  
581 determine whether the FUI is sensitive to the considered perturbations, the FUI  
582 calculated directly from  $R_{rc}(\lambda)$  at MODIS RGB bands were compared with the FUI  
583 calculated from the corresponding  $R_{rs}(\lambda)$  with the same band setting.

584 Figure 16 shows the comparison results for maritime and coastal aerosols at the  
585 scene center and scene edge. The overall relationship between  $R_{rs}$ -based FUI and  $R_{rc}$ -  
586 based FUI under all light conditions is quite robust ( $R^2 = 0.967$ ) with an MRD of 10.9%,  
587 even though the relationship deteriorates a little under coastal aerosols with larger  
588 aerosol optical thickness at 869 nm ( $\tau(869)$ ) towards the scene edge. These  
589 perturbations resulted in 9.5% of the data indicating a different trophic state to that  
590 indicated by the FUI calculated from the original  $R_{rs}(\lambda)$  data. The results illustrate that  
591 the FUI algorithm is generally insensitive to perturbations due to aerosols and

592 observation conditions. This may be because of the normalization process in the  
 593 chromaticity coordinate calculation and the clustering process in the 21-indices  
 594 classification, which may reduce the uncertainties caused by different aerosol types.



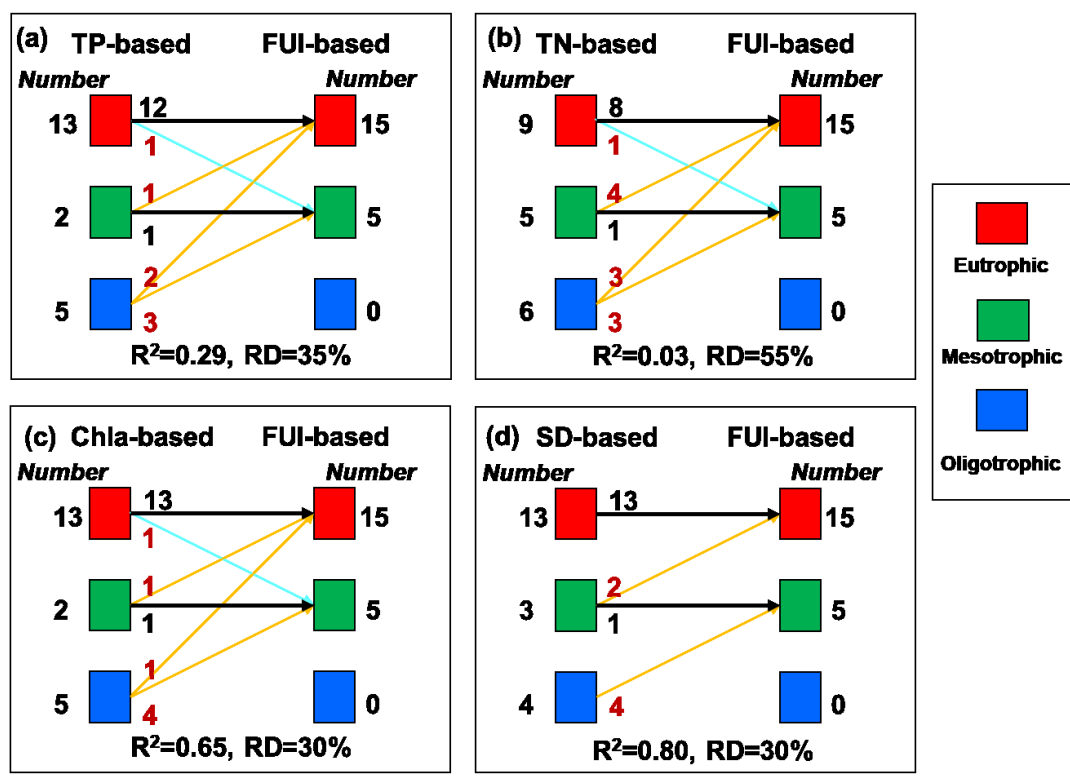
595  
 596 Figure 16 Relationship between  $R_{rc}$ -based FUI and  $R_{rs}$ -based FUI with various atmospheric  
 597 conditions (i.e., aerosol type and optical thickness at 869 nm ( $\tau(869)$ )) and solar/viewing geometry,  
 598 based on model simulations. Two aerosol types were used in the simulations: (a and b) coastal

599 aerosol with 50% relative humidity (C50) and (c and d) maritime aerosol with 90% relative humidity  
600 (M90). Two solar/viewing geometries were performed in the simulations: (a and c) near scene center  
601 and (b and d) near scene edge. (e) Relationship between  $R_{rs}$ -based FUI and  $R_{re}$ -based FUI under all  
602 considered conditions ( $R^2 = 0.967$ , MRD = 10.9%, RMSD = 0.823,  $n = 336$ ). MRD denotes the  
603 mean relative difference and RMSD denotes the root mean square difference.

## 604 **5.2 Relationship between the FUI-based method and traditional trophic state** 605 **assessments**

606 Our FUI-based trophic state assessment method depends on water colour  
607 information derived from satellite imagery, which is in contrast to traditional  
608 assessment methods that depend on one or several biophysical variables (i.e., Chl-a, SD,  
609 TP, TN, COD and biomass; Burns et al., 1999; Vant, 1987). To compare the FUI-based  
610 method with traditional variables, we compared our results with data in the NLA2007  
611 report (USEPA, 2009), which contains both Chl-a based trophic state assessments, and  
612 additional trophic state assessments based on SD, TP, and TN. Using the 20 lakes found  
613 in both datasets, the results showed that the FUI-based classifications were better  
614 correlated with SD and Chl-a ( $R^2 = 0.80, 0.65$ ,  $p < 0.05$ , RD (relative error) = 30%;  
615 Figure 17), reflecting the importance of water clarity and Chl-a in controlling water  
616 colour. The correlation between the FUI-based results and TP-based trophic state  
617 assessments was also strong ( $R^2 = 0.29$ ,  $p < 0.05$ , RD = 35%). However, the TN-based  
618 results had a weak relationship with the FUI-based results ( $R^2 = 0.03$ , RD = 55%).  
619 Similarly, the TN-based results had an insignificant relationship with the Chl-a-based  
620 results ( $R^2 = 0.03$ ), as there is usually a weak relationship between TN and Chl-a in  
621 lakes (Guildford and Hecky, 2000).

622 Of the 20 U.S. lakes compared, none were classified as oligotrophic in the FUI-  
 623 based results (Figure 17), but 5 lakes were classified as oligotrophic in the Chl-a-based  
 624 NLA results. This misclassification of oligotrophic lakes as mesotrophic was also seen  
 625 in the validation comparison data (Table 2), which will be discussed in Section 5.3.



626  
 627 Figure 17 Comparison of lakes classified as different trophic states using the Forel-Ule index (FUI)-  
 628 based trophic state results and National Lake Assessment 2007 (USEPA, 2009) results based on (a)  
 629 total phosphorus (TP), (b) total nitrogen (TN), (c) chlorophyll-a (Chl-a), and (d) Secchi depth (SD),  
 630 for the 20 matched lakes.  $R^2$  denotes the determination coefficient and RD denotes the relative error.

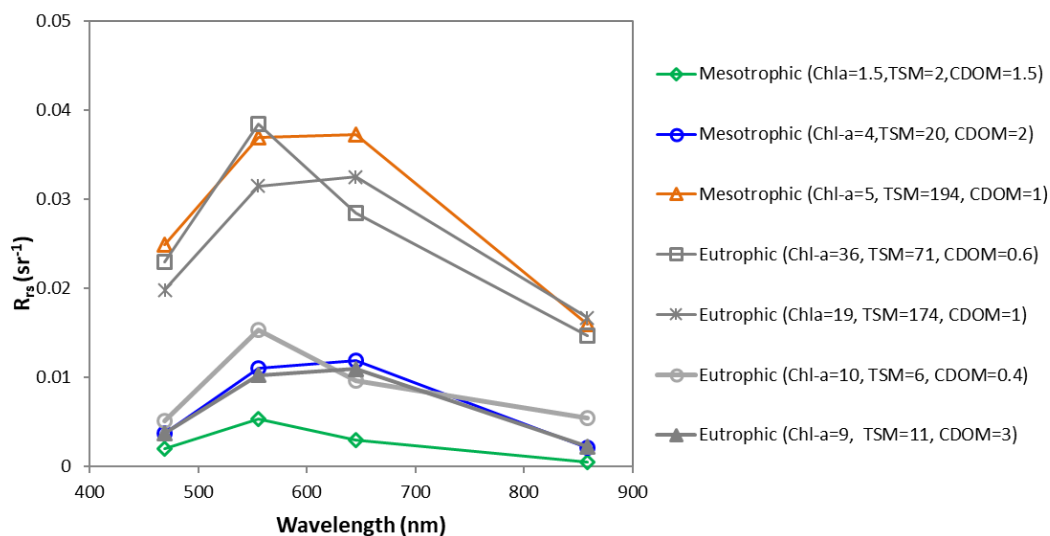
631 **5.3 Uncertainties of trophic state assessment using FUI**

632 Since there is currently no single RS algorithm applicable for the global inland  
 633 waters to retrieve the trophic state related parameters (i.e.Chl-a), as a relatively easy-  
 634 to-produce image product, the FUI-based method makes it possible to assess the trophic  
 635 states of global inland waters. Although the trophic state of the waters across the in-situ

636 dataset and independent dataset could be classified with relatively high accuracy (~80%)  
637 with the FUI, the confusion matrix of the FUI-based classification for 100 investigated  
638 lakes (Table 2) shows that the FUI method led to an over-estimation of the trophic state  
639 of a small proportion of lakes. This may be explained by differences in the division of  
640 the trophic states by different different assessing methods. The trophic state  
641 classification in this study adopted the boundaries of 1 and 7  $\mu\text{g/L}$ , based on Carlson  
642 (1977). However, the USEPA (2016) adopted the boundaries of 2 and 7  $\mu\text{g/L}$ . Hence,  
643 there may be some over-estimation in the mesotrophic state when using the FUI method  
644 because of the lower boundary. The other reason might be that the FUI of waters may  
645 appear larger when there are other optically active constituents in addition to Chl-a that  
646 dominate these optically complex inland waters.

647 We identified the mesotrophic waters from the eutrophic waters with  $\text{FUI} \geq 10$  by  
648 using a red band ( $R_{rs}(645)$ ) threshold method, because the relatively high CDOM  
649 content in water changes the water colour to green and yellow, and the backscattering  
650 of the water in the red band is quite low because of the low TSM content. In the cyan  
651 box in Figure 9, there were a few other situations that result in the misclassification of  
652 mesotrophic waters, which are shown in Figure 17. For these mesotrophic waters with  
653  $\text{FUI} \geq 10$ , the optical properties are generally dominated by abundant CDOM or TSM.  
654 Mesotrophic water dominated by relatively high CDOM and with very low TSM can  
655 be identified from eutrophic water using the red band threshold method. However, for

656 water dominated by high CDOM with relatively high TSM, the  $R_{rs}(\lambda)$  spectra is similar  
 657 to eutrophic waters and cannot be distinguished using the MODIS bands. It is difficult  
 658 to distinguish between mesotrophic and eutrophic waters when dominated by high TSM  
 659 with the MODIS imagery. Further assessment of the trophic state of these two specific  
 660 situations will require platforms with superior spectral resolution.



661  
 662 Figure 17 Different types of water-leaving reflectance ( $R_{rs}(\lambda)$ ) spectra of waters with  $FUI \geq 10$ ,  
 663 including eutrophic and confusing mesotrophic waters. The unit for Chl-a is  $\mu\text{g/L}$ , for TSM is  
 664  $\text{mg/L}$ , for CDOM is  $\text{m}^{-1}$  which means the absorption coefficient at 440 nm.

665 As the summer-average FUI of each water body was used to assess the trophic  
 666 state of the water body, the averaging processes may result in the loss of spatial and  
 667 temporal characteristics of some water bodies, whilst reducing the occurrence of  
 668 unexpected errors and uncertainties. In this case, a water body that is partly eutrophic  
 669 and partly mesotrophic may be classified as mesotrophic after the averaging process.  
 670 The timing of the images also affects the results, as the trophic state of lake may change  
 671 during the summer months. Therefore, a threshold for the number of images of no less

672 than three over the summer months is therefore considered necessary and avoids the  
673 cases where two consecutive images may produce a biased result against the average  
674 state. From the global results, the spatial CV of the water bodies ranged from 0.0% to  
675 41.2% with an average value of 12.9%, and the temporal CV ranged from 0.0% to 54.3%  
676 with an average value of 9.9%. Large variations in these waters might in part be related  
677 to the impact of cloud cover influencing or biasing the pixel coverage for a lake for  
678 different areas, whilst some may also be related to extreme events such as sudden algae  
679 blooms or sediment plumes following heavy rainfall.

680 The data quality of MODIS Terra was often considered not adequate for ocean  
681 colour applications (Franz et al., 2008). But around 2010, NASA started reprocessing  
682 of all the MODIS Terra products and produced good agreement with MODIS Aqua by  
683 using improved radiometric calibration to account for sensor degradation (Li et al.,  
684 2017; Lyapustin et al., 2014; Meister and Franz, 2011). In addition, for inland waters,  
685 the water signal has a greater contribution in the TOA radiance, which tends to be much  
686 greater than that associated with open ocean waters.

687 There may be some uncertainties induced by the calibration of Terra MODIS and  
688 the artefacts of atmospheric correction in the derivation of  $R_{rs}(\lambda)$  and FUI from Terra  
689 MOD09 products in this study. Nevertheless, following the simple water-leaving  
690 reflectance correction, the comparison between MODIS FUI and in-situ derived FUI  
691 and the evaluation of the FUI sensitivity to remaining data perturbations produced good

692 results and demonstrated the validity and practicability of the MOD09 product and the  
693 simple correction method for a wide range of inland waters. As might be expected, the  
694 producer accuracies (Liu et al., 2007) in the confusion matrix (Table 3) for darker waters  
695 like oligotrophic and mesotrophic waters, are relatively low (79.2% and 51.9%). As  
696 described, this is likely associated with calibration errors and artefacts introduced from  
697 atmospheric correction over dark waters (Wang et al., 2016). Hence, for global inland  
698 waters with various optical properties, a more robust atmospheric correction for satellite  
699 products remains a high research priority.

700       Moreover, we chose Terra MOD09 as the main data source rather than Aqua  
701 MYD09 because of the frequent stripe noise. The stripe noise in band 6 (1640 nm) is  
702 severe in the Aqua MYD09 and Aqua MYD02 (the Level-1B Calibrated Geolocation  
703 Data Set), which is induced by the detectors in Aqua MODIS band 6 and has been  
704 reported in numerous studies (Rakwatin et al., 2009; Wang et al., 2006; Doelling et al.,  
705 2015). Band 6 is a useful SWIR band used in this study to detect water areas and  
706 atmospheric noises; however, the stripe noise in this band in Aqua would result in  
707 inaccurate water area masks and water-leaving reflectance.

#### 708       **5.4 Applicability to new satellite sensors**

709       The FUI retrieval algorithms from the water-leaving reflectance spectra have been  
710 established for various satellite sensors such as MODIS, MERIS, Landsat-8 OLI,  
711 Sentinel-3 OLCI (Wang et al., 2015; Wernand et al., 2013; Van der Woerd and Wernand,

712 2015, 2018). There are two main approaches for calculating CIE tristimulus X, Y, Z.  
713 One is to rebuild the spectral data using an interpolation approach (Van der Woerd and  
714 Wernand, 2015, 2018). The other approach is specific to sensors with only RGB bands  
715 in the visible range, and it converts RGB to CIE X, Y, Z using the conversion equation,  
716 as shown in Equation (3) (C.I.E., 1932; Wang et al., 2015). However, despite whether  
717 an interpolation approach or the RGB conversion approach is used, there would be  
718 colour differences from the human eye sensed true colour caused by the band setting of  
719 the sensors (Van der Woerd and Wernand, 2015). To remove this difference, a delta  
720 correction method was introduced by Van der Woerd and Wernand (2015) and adopted  
721 in this study which models the difference between the sensor results and the true colour  
722 results using polynomial fittings. Therefore, with the delta correction, the FUI and the  
723 angle  $\alpha$  calculated can be comparable and transferable between different satellite  
724 sensors (Van der Woerd and Wernand, 2015, 2018). It is notable that the definition for  
725 angle  $\alpha$  enables it increase with FUI in this study, while the definition for angle  $\alpha$  in  
726 Van der Woerd and Wernand (2015) results in a decrease with FUI considering the  
727 different start and revolving direction of angle  $\alpha$  adopted. A transfer is first required  
728 when comparing angle  $\alpha$  derived using the different definitions. Regardless of the  
729 definition of angle  $\alpha$ , the FUI calculated are consistent because the same set of  
730 chromaticity coordinates of the Forel-Ule scales were used (Novoa et al., 2013).  
731 Furthermore, the FUI calculated from new sensors, like Landsat-8 OLI and Sentinel-3

732 OLCI, could be generally comparable with that from MODIS using a proper correction  
733 method for the band settings (Van der Woerd and Wernand, 2018). With recently  
734 launched sensors such as the Landsat-8 OLI and Sentinel-2(A & B), smaller lakes can  
735 be added to the dataset to achieve more comprehensive global results.

## 736 **6. Conclusions**

737 In this study, the trophic states of global large inland waters were assessed using  
738 an FUI-based remote sensing algorithm. The successful outcome can be attributed to  
739 two factors: (1) the water colour index, FUI, can be calculated from MOD09A1 data  
740 with considerable accuracy (~90%) through comparison with in-situ data, and it is  
741 nearly immune to aerosol perturbations and variations in observation conditions. Such  
742 tolerances lead to significantly increased validity, which is critical to FUI's application  
743 on the global scale; (2) The FUI-based trophic state assessment algorithm was  
744 developed based on the analysis of the relationship between FUI and TSI from 469  
745 samples from in-situ measurements at 10 lakes around the world, which contain a wide  
746 range of optical and water quality properties. This led to a robust trophic state  
747 assessment method for inland waters on large scales, and an overall accuracy of 80%  
748 was achieved. This algorithm could be applied to other satellite sensors with the  
749 establishment of FUI retrieval algorithms from various sensors.

750 The assessment algorithm was implemented on MODIS images collected in the  
751 austral and boreal summers of 2012, and the trophic states of the water bodies were

752 classified as oligotrophic, mesotrophic, or eutrophic. Of the 2058 water bodies  
753 considered, eutrophic water bodies accounted for 63.1% of the total number but only  
754 30.5% of the total surface area, mesotrophic water bodies accounted for 26.2% of the  
755 total number and 39.4% of the total surface area, and oligotrophic water bodies  
756 accounted for 10.7% of the total number but 30.1% of the total surface area.  
757 Oligotrophic large lakes were found to be concentrated in plateau regions in Central  
758 Asia and southern South America, while eutrophic large lakes were concentrated in  
759 central Africa, eastern Asia, and mid-northern and southeast North America.

## 760 **Acknowledgements**

761 This research was sponsored by the National Key Research and Development Program  
762 of China (2016YFB0501502), National Natural Science Foundation of China  
763 (41325004, 41471308, and 41671203), Youth Innovation Promotion Association of  
764 Chinese Academy of Sciences (2015128), and China Scholarship Council. We also  
765 gratefully acknowledge the UK NERC GloboLakes project (NE/J024279/1), including  
766 the Limnades data base ([www.limnades.org](http://www.limnades.org)). Moritz Lehmann was funded by grant  
767 UOWX1503 from the New Zealand Ministry for Business, Innovation and  
768 Employment.

## 769 **References**

770 Auer, M. T., Bub, L. A. (2004). Selected features of the distribution of chlorophyll along  
771 the southern shore of Lake Superior. *Journal of Great Lakes Research*, 30, 269-284.  
772 Avery, S., Eng, C. (2012). Lake Turkana & the Lower Omo: hydrological impacts of  
773 major dam and irrigation developments. African Studies Centre, the University of

774 Oxford.

775 Baban, S. M. (1996). Trophic classification and ecosystem checking of lakes using  
776 remotely sensed information. *Hydrological sciences journal*, 41(6), 939-957.

777 Barbiero, R. P., Lesht, B. M., Warren, G. J. (2012). Convergence of trophic state and  
778 the lower food web in lakes huron, michigan and superior. *Journal of Great Lakes  
779 Research*, 38(2), 368-380.

780 Beeton, A. M., Edmondson, W. T. (1972). The eutrophication problem. *Journal of the  
781 Fisheries Board of Canada*, 29(6), 673-682.

782 Bigham Stephens, D. L., Carlson, R. E., Horsburgh, C. A., Hoyer, M. V., Bachmann, R.  
783 W., Canfield Jr, D. E. (2015). Regional distribution of Secchi disk transparency in  
784 waters of the United States. *Lake and Reservoir Management*, 31(1), 55-63.

785 Binding, C. E., Greenberg, T. A., Watson, S. B., Rastin, S., Gould, J. (2015). Long term  
786 water clarity changes in North America's Great Lakes from multi-sensor satellite  
787 observations. *Limnology and Oceanography*, 60(6), 1976-1995.  
788 <http://doi.org/10.1002/lno.10146>.

789 Binding, C. E., T. A. Greenberg, and R. P. Bukata. (2013). The MERIS Maximum  
790 Chlorophyll Index; its merits and limitations for inland water algal bloom  
791 monitoring. *J. Great Lakes Res.* 39: 100–107. doi:10.1016/j.jglr.2013.04.005

792 Bridgeman, T. B., Chaffin, J. D., Filbrun, J. E. (2013). A novel method for tracking  
793 western Lake Erie *Microcystis* blooms, 2002–2011. *Journal of Great Lakes  
794 Research*, 39(1), 83-89.

795 Bukata, P. R., Jerome, J. H., Kondratyev, K. Y., Pozdnyakov, D. (1995). *Optical  
796 Properties and Remote Sensing of Inland and Coastal Waters* Boca Raton: CRC  
797 Press.

798 Bukata, R. P., Bruton, J. E., Jerome, J. H. (1983). Use of chromaticity in remote  
799 measurements of water-quality. *Remote Sensing of Environment*, 13(2), 161-177.

800 Burns, N. M., Bryers, G. (2000). *Protocols for monitoring trophic levels of New  
801 Zealand lakes and reservoirs*. Ministry for the Environment.

802 Burns, N. M., Rutherford, J. C., Clayton, J. S. (1999). A monitoring and classification  
803 system for New Zealand lakes and reservoirs. *Lake and Reservoir Management*,  
804 15(4), 255-271.

805 C.I.E. (1932). *Commission Internationale de l'Eclairage Proceedings 1931*, Cambridge  
806 Univ. Press, 19-29.

807 Carlson, R. E. (1977). A trophic state index for lakes. *Limnology and oceanography*,  
808 22(2), 361-369.

809 Carlson, R. E. (1991). Expanding the trophic state concept to identify non-nutrient  
810 limited lakes and reservoirs. *Enhancing the states's lake management programs*,  
811 59-71.

812 Chaffin, J. D., Bridgeman, T. B., Heckathorn, S. A., Mishra, S. (2011). Assessment of  
813 *Microcystis* growth rate potential and nutrient status across a trophic gradient in  
814 western Lake Erie. *Journal of Great Lakes Research*, 37(1), 92-100.

- 815 Chen, J., Quan, W., Zhang, M., Cui, T. (2013a). A simple atmospheric correction  
816 algorithm for MODIS in shallow turbid waters: A case study in Taihu Lake. *IEEE*  
817 *Journal of Selected Topics in Applied Earth Observations and Remote Sensing*,  
818 6(4), 1825-1833.
- 819 Chen, L. (2003). A study of applying genetic programming to reservoir trophic state  
820 evaluation using remote sensor data. *International Journal of Remote Sensing*,  
821 24(11), 2265-2275.
- 822 Chen, R. (2009). Research on water quality appraisal and water environmental capacity  
823 of Zhelin Reservoir. Master Dissertation. Nanchang University.
- 824 Chen, X., Yang, X., Dong, X., Liu, E. (2013b). Environmental changes in Chaohu Lake  
825 (southeast, China) since the mid-20th century: the interactive impacts of nutrients,  
826 hydrology and climate. *Limnologica-Ecology and Management of Inland Waters*,  
827 43(1), 10-17.
- 828 Cheng, K. S., Lei, T. C. (2001). Reservoir trophic state evaluation using Landsat TM  
829 images. *Journal of the American Water Resources Association*, 37, 1321-1334.
- 830 Chernetskiy, M., Shevyrnogov, A., Shevnina, S., Vysotskaya, G., Sidko, A. (2009).  
831 Investigations of the Krasnoyarsk Reservoir waters based on the multispectral  
832 satellite data. *Advances in Space Research*, 43(2), 206-213.
- 833 Coci, M., Odermatt, N., Salcher, M. M., Pernthaler, J., Corno, G. (2015). Ecology and  
834 distribution of thaumarchaea in the deep hypolimnion of Lake Maggiore. *Archaea-*  
835 *An International Microbiological Journal*, 2015.
- 836 Diaz, M., Pedrozo, F. and Baccala, N. (2000). Summer classification of Southern  
837 Hemisphere temperate lakes (Patagonia, Argentina). *Lakes & Reservoirs: Research*  
838 *& Management*, 5: 213–229.
- 839 Dierssen, H.M., Zimmerman, R.C., Leathers, R.A., Downes, T.V. and Davis, C.O., 2003.  
840 Ocean color remote sensing of seagrass and bathymetry in the Bahamas Banks by  
841 high - resolution airborne imagery. *Limnology and oceanography*, 48(1part2),  
842 pp.444-455.
- 843 Doelling, D. R., Wu, A., Xiong, X., Scarino, B. R., Bhatt, R., Haney, C. O., Gopalan,  
844 A. (2015). The radiometric stability and scaling of collection 6 Terra-and Aqua-  
845 MODIS VIS, NIR, and SWIR spectral bands. *IEEE Transactions on Geoscience*  
846 *and Remote Sensing*, 53(8), 4520-4535.
- 847 Duan, H., Zhang, Y., Zhang, B., Song, K., Wang, Z. (2007). Assessment of chlorophyll-  
848 a concentration and trophic state for Lake Chagan using Landsat TM and field  
849 spectral data. *Environmental monitoring and assessment*, 129(1-3), 295-308.
- 850 Fitzsimmons, K. E., Barrows, T. T. (2010). Holocene hydrologic variability in  
851 temperate southeastern Australia: an example from Lake George, New South Wales.  
852 *The Holocene*, 20(4), 585-597.
- 853 Forsberg, D., Ryding, S. O. (1980). Eutrophication parameters and trophic indices in  
854 30 Swedish lakes. *Arch Hydrobiol.*89:189–207.
- 855 Friedl, M. A., Sulla-Menashe, D., Tan, B., Schneider, A., Ramankutty, N., Sibley, A.,

856 andHuang, X. (2010). MODIS Collection 5 global land cover: Algorithm  
857 refinements and characterization of new datasets. *Remote Sensing of Environment*,  
858 114, 168–182.

859 Fuentes, N., Güde, H., Wessels, M., Straile, D. (2013). Allochthonous contribution to  
860 seasonal and spatial variability of organic matter sedimentation in a deep  
861 oligotrophic lake (Lake Constance). *Limnologica-Ecology and Management of  
862 Inland Waters*, 43(2), 122-130.

863 Garaba, S. P., Badewien, T. H., Braun, A., Schulz, A.-C., Zielinski, O. (2014). Using  
864 ocean colour remote sensing products to estimate turbidity at the Wadden Sea time  
865 series station Spiekeroog. *J. Europ. Opt. Soc. Rap. Public.* 9 (14020): 1-6.

866 Giardino, C., Bresciani, M., Stroppiana, D., Oggioni, A., Morabito, G. (2013). Optical  
867 remote sensing of lakes: an overview on Lake Maggiore. *Journal of Limnology*,  
868 73(s1).

869 Giardino, C., Bresciani, M., Cazzaniga, I., Schenk, K., Rieger, P., Braga, F., et al. (2014).  
870 Evaluation of multi-resolution satellite sensors for assessing water quality and  
871 bottom depth of lake garda. *Sensors*, 14(12), 24116-31

872 Guildford, S.J. and Hecky, R.E., (2000). Total nitrogen, total phosphorus, and nutrient  
873 limitation in lakes and oceans: is there a common relationship?. *Limnology and  
874 Oceanography*, 45(6), 1213-1223.

875 Härmä, P., Vepsäläinen, J., Hannonen, T., Pyhälähti, T., Kämäri, J., Kallio, K. (2001).  
876 Detection of water quality using simulated satellite data and semi-empirical  
877 algorithms in Finland. *Science of the Total Environment*, 268(1), 107-121.

878 Hecky, R. E., Mugidde, R., Ramlal, P. S., Talbot, M. R., Kling, G. W. (2010). Multiple  
879 stressors cause rapid ecosystem change in Lake Victoria. *Freshwater Biology*,  
880 55(s1), 19-42.

881 Holden, H., LeDrew, E. (2002). Measuring and modeling water column effects on  
882 hyperspectral reflectance in a coral reef environment. *Remote Sensing of  
883 Environment*, 81(2), 300-308.

884 Holeck, K. T., Rudstam, L. G., Watkins, J. M., Luckey, F. J., Lantry, J. R., Lantry, B. F.,  
885 Johnson, T. B. (2015). Lake Ontario water quality during the 2003 and 2008  
886 intensive field years and comparison with long-term trends. *Aquatic Ecosystem  
887 Health & Management*, 18(1), 7-17.

888 Hou, X., Feng, L., Duan, H., Chen, X., Sun, D., Shi, K. (2017). Fifteen-year monitoring  
889 of the turbidity dynamics in large lakes and reservoirs in the middle and lower basin  
890 of the Yangtze River, China. *Remote Sensing of Environment*, 190, 107-121.

891 Hu, C., K. L. Carder, and F. E. Muller-Karger. (2000). Atmospheric Correction of  
892 SeaWiFS Imagery over Turbid Coastal Waters: A Practical Method. *Remote  
893 Sensing of Environment* 74: 195–206. doi:10.1016/S0034-4257(00)00080-8.

894 Hu, C., Lee, Z., Ma, R., Yu, K., Li, D., Shang, S. (2010). Moderate resolution imaging  
895 spectroradiometer (MODIS) observations of cyanobacteria blooms in Taihu Lake,  
896 China. *Journal of Geophysical Research: Oceans*, 115(C4).

- 897 Hurlbert, S. H. (Ed.). (2012). Saline Lakes V: Proceedings of the Vth International  
 898 Symposium on Inland Saline Lakes, held in Bolivia, 22–29 March 1991 (Vol. 87).  
 899 Springer Science & Business Media.
- 900 IOCCG (2006). Remote sensing of Inherent Optical Properties: fundamentals, tests of  
 901 algorithms, and applications. Lee, Z.-P. (ed.), Reports of the International Ocean-  
 902 Colour Coordinating Group, No. 5, IOCCG, Dartmouth, Canada.
- 903 Jacobs L L. (1989). Limnological characteristics of big and little minto lakes, Alaska.  
 904 Alaska's hidden resource, 1989: 17.
- 905 Jaquet, J. M., Nirel, P., Martignier, A. (2013). Preliminary investigations on  
 906 picoplankton-related precipitation of alkaline-earth metal carbonates in meso-  
 907 oligotrophic Lake Geneva (Switzerland). *Journal of Limnology*, 72(3), 50.
- 908 Jin, X. C., Tu, Q. Y. (1990). The standard methods for observation and analysis in lake  
 909 eutrophication. Chinese Environmental Science Press, Beijing, 240.
- 910 Jones, R. A., Lee, G. F. (1982). Recent advances in assessing impact of phosphorus  
 911 loads on eutrophication-related water quality. *Water Research*, 16(5), 503-515.
- 912 Joniak, T., Nagengast, B., Kuczynska-Kippin, N. (2009). Can popular systems of  
 913 trophic classified be used for small water bodies? *Oceanological and*  
 914 *hydrobiological studies. International Journal of oceanography and hydrobiology*,  
 915 XXXVIII(4), 145–151
- 916 Khandelwal, A., Karpatne, A., Marlier, M. E., Kim, J., Lettenmaier, D. P., Kumar, V.  
 917 (2017). An approach for global monitoring of surface water extent variations in  
 918 reservoirs using MODIS data. *Remote Sensing of Environment*.
- 919 Kingston, John. (2015). Completion Report Mille Lacs Lake Paleolimnology Project.  
 920 <http://hdl.handle.net/10792/1832>.
- 921 Klein, I., Gessner, U., Dietz, A. J., Kuenzer, C. (2017). Global WaterPack—A 250 m  
 922 resolution dataset revealing the daily dynamics of global inland water bodies.  
 923 *Remote Sensing of Environment*, 198, 345-362.
- 924 Knight, J. F., Voth, M. L. (2012). Application of MODIS imagery for intra-annual water  
 925 clarity assessment of Minnesota lakes. *Remote Sensing*, 4(7), 2181-2198.
- 926 Kshitij Mishra and P. Rama Chandra Prasad. (2015). Automatic extraction of water  
 927 bodies from Landsat imagery using Perceptron model, *Journal of Computational*  
 928 *Environmental Sciences*, vol. 2015, Article ID 903465, 9 pages, 2015.  
 929 doi:10.1155/2015/903465
- 930 Kutser, T., E. Vahtm ae, B. Paavel, and T. Kauer. (2013). Removing glint effects from  
 931 field radiometry data measured in optically complex coastal and inland waters.  
 932 *Remote Sens. Environ.* 133: 85–89. doi:10.1016/j.rse.2013.02.011
- 933 Landis, J. R., Koch, G. G. (1977). An application of hierarchical kappa-type statistics  
 934 in the assessment of majority agreement among multiple observers. *Biometrics*,  
 935 363-374.
- 936 Le, C., Zha, Y., Li, Y., Sun, D., Lu, H., Yin, B. (2010). Eutrophication of lake waters in  
 937 China: cost, causes, and control. *Environmental Management*, 45(4), 662-668.

938 Lee, Z., Carder, K. L., Mobley, C. D., Steward, R. G., Patch, J. S. (1998). Hyperspectral  
939 remote sensing for shallow waters. I. A semianalytical model. *Applied optics*,  
940 37(27), 6329-6338.

941 Lehner, B., Döll, P. (2004). *Global Lakes and Wetlands Database GLWD*. GLWD Docu-  
942 mentation.

943 Li J., Wu D., Wu Y., Liu H., Shen Q., Zhang H. (2009). Identification of algae-bloom  
944 and aquatic macrophytes in Lake Taihu from in-situ measured spectra data. *Journal*  
945 *of Lake Sciences*, 21(2), 215-222.

946 Li, J., Wang, S., Wu, Y., Zhang, B., Chen, X., Zhang, F., Shen, Q., Peng, D., Tian, L.  
947 (2016). MODIS observations of water color of the largest ten lakes in China  
948 between 2000 and 2012. *International Journal of Digital Earth*, 1-18.

949 Lillesand, T. M., Johnson, W. L., Deuell, R. L., Lindstrom, O. M., Meisner, D. E. (1983).  
950 Use of Landsat data to predict the trophic state of Minnesota lakes.

951 Lim, A., Hedley, J. D., LeDrew, E., Mumby, P. J., Roelfsema, C. (2009). The effects of  
952 ecologically determined spatial complexity on the classification accuracy of  
953 simulated coral reef images. *Remote Sensing of Environment*, 113(5), 965-978.

954 Liu, C., Frazier, P., Kumar, L. (2007). Comparative assessment of the measures of  
955 thematic classification accuracy. *Remote sensing of environment*, 107(4), 606-616.

956 Lyzenga, D. R. (1978). Passive remote sensing techniques for mapping water depth and  
957 bottom features. *Applied optics*, 17(3), 379-383.

958 Ma, S., Tao, Z., Yang, X., Yu, Y., Zhou, X., Li, Z. (2014). Bathymetry retrieval from  
959 hyperspectral remote sensing data in optical-shallow water. *IEEE Transactions on*  
960 *Geoscience and Remote Sensing*, 52(2), 1205-1212.

961 Matthews, M. W., Odermatt, D. (2015). Improved algorithm for routine monitoring of  
962 cyanobacteria and eutrophication in inland and near-coastal waters. *Remote*  
963 *Sensing of Environment*, 156, 374-382.

964 McClain, C. R. (2009). A decade of satellite ocean color observations\*. *Annual Review*  
965 *of Marine Science*, 1, 19-42.

966 Ministry of Environmental Protection of the People's Republic of China (MEPPRC).  
967 2013. China Environmental State Bulletin 2012.  
968 <http://jcs.mep.gov.cn/hjzl/zkgb/2012zkgb/>.

969 Mobley, C. D., Sundman, L. K. (2003). Effects of optically shallow bottoms on  
970 upwelling radiances: Inhomogeneous and sloping bottoms. *Limnology and*  
971 *Oceanography*, 48(1part2), 329-336.

972 Mukherjee, M., Ray, A., Post, A. F., McKay, R. M., Bullerjahn, G. S. (2016).  
973 Identification, enumeration and diversity of nitrifying planktonic archaea and  
974 bacteria in trophic end members of the Laurentian Great Lakes. *Journal of Great*  
975 *Lakes Research*, 42(1), 39-49.

976 Okullo, W., Hamre, B., Frette, Ø, Stamnes, J. J., Sørensen, K., Ssenyonga, T. (2011).  
977 Validation of MERIS water quality products in Murchison bay, Lake Victoria–  
978 preliminary results. *International journal of remote sensing*, 32(19), 5541-5563.

- 979 Olmanson, L. G., Bauer, M. E., Brezonik, P. L. (2008). A 20-year Landsat water clarity  
980 census of Minnesota's 10,000 lakes. *Remote Sensing of Environment*, 112(11),  
981 4086-4097.
- 982 O'Reilly, C. M., Alin, S. R., Plisnier, P. D., Cohen, A. S., McKee, B. A. (2003). Climate  
983 change decreases aquatic ecosystem productivity of Lake Tanganyika, Africa.  
984 *Nature*, 424(6950), 766-768.
- 985 O'Reilly, J.E., Maritorena, S., Mitchell, B. G., Siegel, D. A., Carder, K. L., Garver, S.  
986 A., Kahru, M., McClain, C. R. (1998). Ocean color chlorophyll algorithms for  
987 SeaWiFS, *Journal of Geophysical Research* 103, 24937-24953, doi:  
988 10.1029/98JC02160.
- 989 Palmer, S. C. J., Kutser, T., Hunter, P. D. (2015). Remote sensing of inland waters:  
990 Challenges, progress and future directions. *Remote Sensing of Environment*, 157,  
991 1-8. doi:10.1016/j.rse.2014.09.021
- 992 Papoutsas, C., Akylas, E., Hadjimitsis, D. (2014). Trophic State Index derivation through  
993 the remote sensing of Case-2 water bodies in the Mediterranean Region. *Open*  
994 *Geosciences*, 6(1), 67-78.
- 995 Pulliainen, J., Kallio, K., Eloheimo, K., Koponen, S., Servomaa, H., et al. (2001). A  
996 semi-operative approach to lake water quality retrieval from remote sensing data.  
997 *Science of the Total Environment*, 268(1), 79-93.
- 998 Raji, A. (1993). The past history and present trends in the fisheries of Lake Chad. 213-  
999 225.
- 1000 Rakwatin, P., Takeuchi, W., Yasuoka, Y. (2009). Restoration of Aqua MODIS band 6  
1001 using histogram matching and local least squares fitting. *IEEE Transactions on*  
1002 *Geoscience and Remote Sensing*, 47(2), 613-627.
- 1003 Rimet, F., Bouchez, A., Montuelle, B. (2015). Benthic diatoms and phytoplankton to  
1004 assess nutrients in a large lake: Complementarity of their use in Lake Geneva  
1005 (France–Switzerland). *Ecological Indicators*, 53, 231-239.
- 1006 Rodhe, W. (1969). Crystallization of eutrophication concepts in northern Europe.
- 1007 Sass, G. Z., Creed, I. F., Bayley, S. E., Devito, K. J. (2007). Understanding variation in  
1008 trophic status of lakes on the Boreal Plain: a 20 year retrospective using Landsat  
1009 TM imagery. *Remote Sensing of Environment*, 109(2), 127-141.
- 1010 Shanmugam, P., Ahn, Y. (2007). New Atmospheric Correction Technique to Retrieve  
1011 the Ocean Colour from Seawifs Imagery in Complexcoastal Waters. *Journal of*  
1012 *Optics A: Pure and Applied Optics* 9: 511–530. doi:10.1088/1464-4258/9/5/016.
- 1013 Sheela, A. M., Letha, J., Joseph, S. (2011b). Environmental status of a tropical lake  
1014 system. *Environmental monitoring and assessment*, 180(1-4), 427-449.
- 1015 Sheela, A. M., Letha, J., Joseph, S., Ramachandran, K. K., Sanalkumar, S. P. (2011a).  
1016 Trophic state index of a lake system using IRS (P6-LISS III) satellite imagery.  
1017 *Environmental monitoring and assessment*, 177(1-4), 575-592.
- 1018 Shen, Q., Li, J. S., Wu, Y. H., Zhang, B. (2014). Review of spectral curve fitting and  
1019 analysis of inherent optical parameters in lakes. *Remote Sensing Information*, 29

1020 (4): 112-125.

1021 Sheng, H., Wu, Z., Liu, M., et al. (2015). Water quality trends in recent 10 years and  
1022 correlation with hydro-meteorological factors in Xin'anjiang Reservoir. *Acta*  
1023 *Scientiae Circumstantiae*, 35(1): 118-127.

1024 Shi, K., Zhang, Y., Zhu, G., Liu, X., Zhou, Y., Xu, H., et al. (2015). Long-term remote  
1025 monitoring of total suspended matter concentration in Lake Taihu using 250m  
1026 MODIS-Aqua data. *Remote Sensing of Environment*, 164, 43-56.

1027 Shi, W., Wang M. (2009). An assessment of the black ocean pixel assumption for  
1028 MODIS SWIR bands. *Remote sensing of environment* 113(8): 1587-1597.

1029 Shuchman, R. A., Leshkevich, G., Sayers, M. J., Johengen, T. H., Brooks, C. N.,  
1030 Pozdnyakov, D. (2013). An algorithm to retrieve chlorophyll, dissolved organic  
1031 carbon, and suspended minerals from Great Lakes satellite data. *Journal of Great*  
1032 *Lakes Research*, 39, 14-33.

1033 Singh, S.P. and Singh, P. (2015). Effect of temperature and light on the growth of algae  
1034 species: a review. *Renewable and Sustainable Energy Reviews*, 50, pp.431-444.

1035 Smith, V. H. (2003). Eutrophication of freshwater and coastal marine ecosystems a  
1036 global problem. *Environmental Science and Pollution Research*, 10(2): 126-139.

1037 Song, K., Ma, J., Wen, Z., Fang, C., Shang, Y., Zhao, Y., Du, J. (2017). Remote  
1038 estimation of  $K_d$  (PAR) using MODIS and Landsat imagery for turbid inland  
1039 waters in Northeast China. *ISPRS Journal of Photogrammetry and Remote Sensing*,  
1040 123, 159-172.

1041 Spyrakos, E., O'Donnell, R., Hunter, P.D., Miller, C., Scott, M., Simis, S.G., Neil, C.,  
1042 Barbosa, C.C., Binding, C.E., Bradt, S. and Bresciani, M. (2018). Optical types of  
1043 inland and coastal waters. *Limnology and Oceanography*, 63(2), pp.846-870.

1044 Stich, H. B., Brinker, A. (2010). Oligotrophication outweighs effects of global warming  
1045 in a large, deep, stratified lake ecosystem. *Global Change Biology*, 16(2), 877-888.

1046 Strahler, A., Muchoney, D., Borak, J., Friedl, M., Gopal, S., Lambin, E., Moody, A.,  
1047 (1999). MODIS Land Cover Product: Algorithm Theoretical Basis Document  
1048 (ATBD), Version 5.0. Boston University, Boston, MA, 72 p.

1049 Stuart H. Hurlbert. (1991). Saline Lakes V, Proceedings of the Vth International  
1050 Symposium on Inland Saline Lakes, held in Bolivia, 22–29 March 1991.

1051 Tang, J. W., Tian, G. L., Wang, X. Y., Wang, X. M., Song, Q. J. (2004). The methods of  
1052 water spectra measurement and analysis I: above-water method. *Journal of Remote*  
1053 *Sensing*, 8(1), 37-44.

1054 Thiemann, S., Kaufmann, H. (2000). Determination of chlorophyll content and trophic  
1055 state of lakes using field spectrometer and IRS-1C satellite data in the Mecklenburg  
1056 Lake District, Germany. *Remote Sensing of Environment*, 73(2), 227-235.

1057 USEPA. (2009). National Lakes Assessment: A collaborative survey of the Nation's  
1058 Lakes. EPA 841-R-09-001. U.S. Environmental Protection Agency, Office of Water  
1059 and Office of Research and Development, Washington, D.C.  
1060 <https://nationallakesassessment.epa.gov/>

1061 USEPA. (2016). National Lakes Assessment 2012: A collaborative survey of lakes in  
1062 the United States. EPA 841-R-16-113. U.S. Environmental Protection Agency,  
1063 Washington, DC. <https://nationallakesassessment.epa.gov/>

1064 Vant, W. N. (Ed.). (1987). Lake managers handbook: a guide to undertaking and  
1065 understanding investigations into lake ecosystems, so as to assess management  
1066 options for lakes (No. 103). Published for the National Water and Soil Conservation  
1067 Authority by the Water and Soil Directorate, Ministry of Works and Development.

1068 Velpuri, N. M., Senay, G. B., Asante, K. O. (2012). A multi-source satellite data  
1069 approach for modelling Lake Turkana water level: calibration and validation using  
1070 satellite altimetry data. *Hydrology and Earth System Sciences*, 16(1), 1-18.

1071 Verburg, P. (2006). The need to correct for the Suess effect in the application of  $\delta^{13}C$   
1072 in sediment of autotrophic Lake Tanganyika, as a productivity proxy in the  
1073 Anthropocene. *Journal of Paleolimnology*, 37(4): 591-602.

1074 Verburg, P., Hamill, K., Unwin, M., Abell, J. (2010). Lake water quality in New Zealand  
1075 2010: Status and trends. NIWA client report HAM, 107.

1076 Vermote, E., Vermeulen A. (1999). Atmospheric correction algorithm: spectral  
1077 reflectances (MOD09), ATBD version 4. [https://eosps0.gsfc.nasa.gov/sites/default/files/atbd/atbd\\_mod08.pdf](https://eosps0.gsfc.nasa.gov/sites/default/files/atbd/atbd_mod08.pdf). (Accessed April 1999).

1079 Vermote, E. F., Roger, J. C., Ray, J. P. (2015). MODIS Surface Reflectance User's  
1080 Guide-Collection 6. In Tech. Rep. Version 1.4, NASA GSFC Terrestrial  
1081 Information Systems Laboratory, MODIS Land Surface Reflectance Science  
1082 Computing Facility. Greenbelt, USA.

1083 Vollenweider, R. A. (1981). Eutrophication- a Global Problem. *Water Qual. Bull.*, 6(3),  
1084 59-62.

1085 Vollenweider, R. A., Kerekes, J. (1982). Eutrophication of waters. Monitoring,  
1086 assessment and control. Organization for Economic Co-Operation and  
1087 Development (OECD), Paris, 156.

1088 Wang, L., Qu, J. J., Xiong, X., Hao, X., Xie, Y., Che, N. (2006). A new method for  
1089 retrieving band 6 of Aqua MODIS. *IEEE Geoscience and Remote Sensing Letters*,  
1090 3(2), 267-270.

1091 Wang, M., and W. Shi. (2007). The NIR-SWIR Combined Atmospheric Correction  
1092 Approach for MODIS Ocean Color Data Processing. *Optics Express* 15: 15722–  
1093 15733. doi:10.1364/OE.15.015722.

1094 Wang, M., Shi, W., Tang, J. (2011). Water property monitoring and assessment for  
1095 China's inland Lake Taihu from MODIS-Aqua measurements. *Remote Sensing of*  
1096 *Environment*, 115(3), 841-854.

1097 Wang, S. M., Dou, H. S. (1998). *Chinese Lakes*. Science Press, Beijing.

1098 Wang, S., Li, J., Shen, Q., Zhang, B., Zhang, F., Lu, Z. (2015). MODIS-based  
1099 radiometric color extraction and classification of inland water with the Forel-Ule  
1100 Scale: A Case Study of Lake Taihu. *IEEE Journal of Selected Topics in Applied*  
1101 *Earth Observations and Remote Sensing*, 8(2), 907-918.

- 1102 Wang, S., Li, J., Zhang, B., Shen, Q., Zhang, F., Lu, Z. (2016). A simple correction  
1103 method for the MODIS surface reflectance product over typical inland waters in  
1104 China, *International Journal of Remote Sensing*, 37:24, 6076-6096.
- 1105 Wang, Z., Hong, J., Du, G. (2008). Use of satellite imagery to assess the trophic state  
1106 of Miyun Reservoir, Beijing, China. *Environmental Pollution*, 155(1), 13-19.
- 1107 Wernand, M. R., Van der Woerd, H. J. (2010). Spectral analysis of the Forel-Ule Ocean  
1108 colour comparator scale. *Journal of the European Optical Society-Rapid*  
1109 *Publications*, 5.
- 1110 Wernand, M. R., Hommersom, A., Van der Woerd, H. J. (2013a). MERIS-based ocean  
1111 colour classification with the discrete Forel-Ule scale. *Ocean Science* 9: 477-487.
- 1112 Wernand, M.R., Van der Woerd, H.J., Gieskes, W.W.C. (2013b). Trends in Ocean  
1113 Colour and Chlorophyll Concentration from 1889 to 2000, Worldwide. *PLoS ONE*  
1114 8(6): e63766. doi:10.1371/journal.pone.0063766
- 1115 Williams, W. (2002). Environmental threats to salt lakes and the likely status of inland  
1116 saline ecosystems in 2025. *Environmental Conservation*, 29(2), 154-167.  
1117 doi:10.1017/S0376892902000103
- 1118 Van der Woerd, H. J., Wernand, M. R. (2015). True colour classification of natural  
1119 waters with medium-spectral resolution satellites: SeaWiFS, MODIS, MERIS and  
1120 OLCI. *Sensors*, 15(10), 25663-25680.
- 1121 Van der Woerd H.J. et al., (2016). True color analysis of natural waters with SeaWiFS,  
1122 MODIS, MERIS and OLCI by SNAP. Presented at Ocean Optics conference, At  
1123 Victoria BC Canada, Volume: XXIII.
- 1124 Wu, G., Cui, L., He, J., Duan, H., Fei, T., Liu, Y. (2013). Comparison of MODIS-based  
1125 models for retrieving suspended particulate matter concentrations in Poyang Lake,  
1126 China. *International Journal of Applied Earth Observation and Geoinformation*, 24,  
1127 63-72.
- 1128 Wu, G., De Leeuw, J., Skidmore, A. K., Prins, H. H., Liu, Y. (2008). Comparison of  
1129 MODIS and Landsat TM5 images for mapping tempo-spatial dynamics of Secchi  
1130 disk depths in Poyang Lake National Nature Reserve, China. *International Journal*  
1131 *of Remote Sensing*, 29(8), 2183-2198.
- 1132 Xiang, B., Song, J. W., Wang, X. Y., Zhen, J. (2015). Improving the accuracy of  
1133 estimation of eutrophication state index using a remote sensing data-driven method:  
1134 A case study of Chaohu Lake, China. *Water SA*, 41(5), 753-761.
- 1135 Yang, L., Lei, K., Meng, W., Fu, G., Yan, W. (2013). Temporal and spatial changes in  
1136 nutrients and chlorophyll- $\alpha$  in a shallow lake, Lake Chaohu, China: An 11-year  
1137 investigation. *Journal of Environmental Sciences*, 25(6), 1117-1123.
- 1138 Ylöstalo, P., Kallio, K., Seppälä, J. (2014). Absorption properties of in-water  
1139 constituents and their variation among various lake types in the boreal region.  
1140 *Remote Sensing of Environment*, 148, 190-205.
- 1141 Zhang, F., Li, J., Zhang, B., Shen, Q., Ye, H., Wang, S., Lu, Z. (2018). A simple  
1142 automated dynamic threshold extraction method for the classification of large

1143 water bodies from landsat-8 OLI water index images. *International Journal of*  
1144 *Remote Sensing*, 39(11), 3429-3451.  
1145 Zhang, M., R. Ma, J. Li, B. Zhang, and H. Duan. (2014). A Validation Study of an  
1146 Improved SWIR Iterative Atmospheric Correction Algorithm for MODIS-Aqua  
1147 Measurements in Lake Taihu, China. *IEEE Transactions on Geoscience and*  
1148 *Remote Sensing* 52 (8): 4686–4695. doi:10.1109/TGRS.2013.2283523.